

# The stellar photosphere-hydrogen ionization front interaction in Classical Pulsators: a theoretical explanation for observed period-colour relations

Susmita Das<sup>1\*</sup>, Shashi M. Kanbur<sup>2</sup>, Earl P. Bellinger<sup>3†</sup>, Anupam Bhardwaj<sup>4‡</sup>,  
Harinder P. Singh<sup>1</sup>, Brett Meerdink<sup>2</sup>, Nicholas Proietti<sup>2</sup>, Anthony Chalmers<sup>2</sup>, and  
Ryan Jordan<sup>2</sup>

1. Department of Physics & Astrophysics, University of Delhi, Delhi 110007, India

2. Department of Physics, State University of New York Oswego, Oswego, NY 13126, USA

3. Stellar Astrophysics Centre, Department of Physics and Astronomy, Aarhus University, Aarhus 8000, Denmark

4. Kavli Institute for Astronomy and Astrophysics, Peking University, Yi He Yuan Lu 5, Hai Dian District, Beijing 100871, China

Accepted 2020 January 17. Received 2020 January 17; in original form 2019 November 15

## ABSTRACT

Period-colour and amplitude-colour (PCAC) relations can be used to probe both the hydrodynamics of outer envelope structure and evolutionary status of Cepheids and RR Lyraes. In this work, we incorporate the PCAC relations for RR Lyraes, BL Her, W Vir and classical Cepheids in a single unifying theory that involves the interaction of the hydrogen ionization front (HIF) and stellar photosphere and the theory of stellar evolution. PC relations for RR Lyraes and classical Cepheids using OGLE-IV data are found to be consistent with this theory: RR Lyraes have shallow/sloped relations at minimum/maximum light whilst long-period ( $P > 10$  days) Cepheids exhibit sloped/flat PC relations at minimum/maximum light. The differences in the PC relations for Cepheids and RR Lyraes can be explained based on the relative location of the HIF and stellar photosphere which changes depending on their position on the HR diagram. We also extend our analysis of PCAC relations for type II Cepheids in the Galactic bulge, LMC and SMC using OGLE-IV data. We find that BL Her stars have sloped PC relations at maximum and minimum light similar to short-period ( $P < 10$  days) classical Cepheids. W Vir stars exhibit sloped/flat PC relation at minimum/maximum light similar to long-period classical Cepheids. We also compute state-of-the-art 1D radiation hydrodynamic models of RR Lyraes, BL Her and classical Cepheids using the radial stellar pulsation code in MESA to further test these ideas theoretically and find that the models are generally consistent with this picture. We are thus able to explain PC relations at maximum and minimum light across a broad spectrum of variable star types.

**Key words:** stars: variables: Cepheids, stars: variables: RR Lyrae, stars: Population II, stars: evolution, Galaxy: bulge, galaxies: Magellanic Clouds

## 1 INTRODUCTION

RR Lyraes, classical Cepheids and Type II Cepheids (T2Cs) are well-known classical pulsators in different evolutionary stages. While RR Lyraes are horizontal-branch stars with helium-burning cores (Preston 1964), classical Cepheids are located on the blue loops in the HR diagram (Anderson et al. 2016). T2Cs are old, low-

mass ( $\sim 0.5 - 0.6 M_{\odot}$ ), metal-poor pulsating variables with typical periods of about 1 to 50 days (Wallerstein 2002; Sandage & Tammann 2006). T2Cs are fainter than the classical Cepheids but brighter than the RR Lyrae stars. They have traditionally been divided into three subclasses: BL Her stars with periods between 1–4 days, W Vir stars with periods ranging from 4–20 days and RV Tau stars with periods longer than 20 days (Soszyński et al. 2018). We note here that RV Tau variables are post AGB stars with typical masses of  $\sim 0.7 M_{\odot}$  (Tuchman et al. 1993; Fokin 1994), higher than those for BL Her and W Vir stars. In addition, there is a fourth subclass, the peculiar W Vir (pW Vir) stars which are brighter and bluer than the W Vir stars (Soszyński et al. 2008). All these classi-

\* E-mail: susmitadas130@gmail.com (SD); shashi.kanbur@oswego.edu (SMK)

† SAC Postdoctoral Fellow

‡ KIAA Postdoctoral Fellow

cal pulsating stars follow well-defined Period-Luminosity relations (PLRs) which make them excellent distance indicators (Muraveva et al. 2015; Bhardwaj et al. 2016a, 2017a; Ripepi et al. 2017; Subramanian et al. 2017; Beaton & Carnegie-Chicago Hubble Program Team 2018).

The PCAC relations for classical Cepheids and RR Lyraes have been extensively studied to understand the hydrodynamics in their outer envelopes (Simon et al. 1993; Kanbur et al. 2004; Bhardwaj et al. 2014; Ngeow et al. 2017; Das et al. 2018). RR Lyrae stars are on the Horizontal Branch (HB) and evolve towards higher luminosities and cooler temperatures in the HR diagram. However, depending on the morphology of the evolutionary tracks, RR Lyraes can evolve bluewards from a relatively red zero-age HB before turning redwards towards the AGB. Their period-colour (PC) relations have a particular structure: shallow/steep sloped relations at minimum/maximum light respectively. Classical Cepheids lie in a region of higher luminosities and cooler temperatures on the HR diagram with respect to the RR Lyrae stars: their PC relations at minimum (steep slope) and maximum (shallow slope) light are the opposite of RR Lyraes. Kanbur et al. (2004); Bhardwaj et al. (2014); Ngeow et al. (2017) and references therein contend that the changes in the PCAC relations are caused by an interaction of the stellar photosphere and hydrogen ionization front (HIF) in the outer envelope. The photosphere is taken as being at optical depth  $\tau = 2/3$  and the HIF is defined where the majority of hydrogen becomes ionized. However, PCAC relations for T2Cs at the maximum and minimum light have not been studied previously.

The classical picture of the theory of stellar evolution suggests that the progenitors of T2Cs evolve redward from the blue edge of the HB and may move up the Asymptotic Giant Branch (AGB) going through the BL Her-type and W Vir-type pulsation stages (Gingold 1985; Wallerstein 2002). However, recent work by Gezer et al. (2015); Groenewegen & Jurkovic (2017a,b); Manick et al. (2017) among others questions this classical picture and the origin and evolution of T2Cs is not as well-understood as was once thought to be. Iwanek et al. (2018) confirmed BL Her stars to be as old as RR Lyraes while W Vir stars could be a mixture of old and intermediate-age stars. While Groenewegen & Jurkovic (2017a) found that BL Her stars may be explained by low-mass stars ( $\sim 0.5 - 0.6M_{\odot}$ ) evolving off the zero-age HB, they state that the evolutionary status of W Vir stars is unclear. This is because for the same luminosity, W Vir stars have longer periods and thus, lower masses than their short period classical Cepheid counterparts. However, evolutionary tracks of  $\sim 2.5 - 4M_{\odot}$  stars cross the W Vir region in the HR diagram. Groenewegen & Jurkovic (2017a) suggested that the origin of W Vir stars may have some relation to binarity.

From the theoretical perspective, several linear and nonlinear convective models for RR Lyraes, Cepheids and T2Cs have been computed to study their pulsation properties and PLRs (Fiorentino et al. 2007; Marconi & Di Criscienzo 2007; Smolec et al. 2012; Marconi et al. 2013, 2015; Bono et al. 2016; Smolec 2016). In the case of Cepheids and RR Lyraes, their light curve structures have also been compared with observations (Bhardwaj et al. 2017b; Das et al. 2018). For T2Cs, Marconi & Di Criscienzo (2007); Smolec (2016) have employed non-linear models to investigate their pulsation modes. While they pulsate primarily in the fundamental mode, double-mode and overtone-mode T2Cs have also been found by Smolec et al. (2018) and Soszyński et al. (2019), respectively. Recently, *Modules for Experiments in Stellar Astrophysics* (MESA, Paxton et al. 2011, 2013, 2015, 2018, 2019) incorporated radial stellar pulsation modules which can be used to generate light curves

of these classical pulsators. Our aim is to compare the observed PCAC relations for RR Lyraes, classical Cepheids and T2Cs with a self-consistent set of pulsation models and relate the empirical variations to changes in the envelope structure and evolutionary states of these variables.

There are several reasons for comparing observed and theoretical PCAC relations. Firstly, PC relations at mean light are important in a wider astrophysical context because through the period-luminosity-colour (PLC) relations, they influence the PLRs which is vital for the distance scale and non-CMB estimates of Hubble’s constant (Beaton et al. 2016; Riess et al. 2016, 2019). Traditionally, PC relations are studied at *mean* light (Tammann et al. 2003) but these relations are the average of the corresponding relations at various phase points during a pulsation cycle. Therefore in order to fully understand the physics behind these relations at mean light, it is important to study such relations during the pulsation cycle. Previous work has found small nonlinearities in the Cepheid PLRs (Bhardwaj et al. 2016b) which may occur due to the significant variations in the PC relation at maximum and minimum light. Further, observed PCAC relations can be compared to theoretical PCAC relations obtained from extensive grids of theoretical pulsation models to constrain global stellar parameters (Bellinger et al. 2019) and hence constrain theories of stellar pulsation and evolution.

Here we focus on PC relations at maximum and minimum light and corresponding AC relations (Bhardwaj et al. 2014; Das et al. 2018, and references therein) because the behaviour at these phases has been shown to be strongly influenced by the interaction between the HIF and the stellar photosphere. In previous work, Simon et al. (1993); Kanbur (1995); Kanbur & Phillips (1996) investigated how such interactions can strongly influence the behavior of PC relations at maximum (classical Cepheids) and minimum light (RR Lyraes). Later Kanbur et al. (2004); Kanbur & Ngeow (2006); Kanbur et al. (2007) modelled this interaction using 1D radiation hydrodynamic models of Cepheids and RR Lyraes. These authors found that the stellar photosphere and the HIF are not always co-moving during a pulsation cycle. When the two are “engaged” (that is, the photosphere lies at the base of the HIF or the distance between them is small) at low temperatures, the temperature of the photosphere takes on the properties of the temperature at which hydrogen ionizes. From Saha ionization equilibrium theory, this temperature is independent of density at low temperatures, leading to a PC relation that is flatter or more independent of global stellar pulsation properties. This is the situation, for example, for Cepheids at maximum light. At minimum light for Cepheids, the photosphere and the HIF are not engaged and the temperature of the photosphere is dependent on global stellar properties - hence we have a sloped PC relation. In the case of RR Lyraes, the photosphere and the HIF are engaged through the pulsation cycle (Kanbur 1995; Kanbur & Phillips 1996). However the interaction is at low temperatures at minimum light and hence RR Lyraes exhibit a flat PC relation at minimum light. At maximum light, this interaction is at higher temperatures and the temperature at which hydrogen ionizes or the temperature of the stellar photosphere is strongly dependent on temperature and global stellar properties. Hence we have a definite slope for RRab PC relations at maximum light but a flat PC slope at minimum light.

One measure of “engagement” between the photosphere and HIF is the distance between them in mass coordinates (Kanbur et al. 2007, and references therein). In this work, we study how this distance varies across classical Cepheids, RR Lyraes and T2Cs and across pulsation phases. We emphasize here that for the purpose

of this paper, the locations of different types of variable stars on the HR diagram and thus, in different evolutionary states determine the relative location of HIF and photosphere. A higher  $L/M$  ratio and/or a cooler effective temperature indicates greater distance between the HIF and the stellar photosphere (Kanbur 1995; Kanbur & Phillips 1996). W Vir stars lie in the same region of the HR diagram as classical Cepheids. The HIF-stellar photosphere interaction theory (Kanbur 1995; Kanbur & Phillips 1996) implies that as a consequence of stellar evolution and because of similar locations of W Vir stars and classical Cepheids on the HR diagram, the PC relation obeyed by W Vir stars should be similar to that for classical Cepheids. We also note that previous work has found some statistically significant differences in PCAC relations between the Galaxy, LMC and SMC, though the general nature (that is, flat PC relation at maximum/minimum for Cepheids/RR Lyraes) is preserved. Hence it is important to understand the effect of metallicity with a view to using such observed PC relations at multiple phases to constrain models. It is in this context that we study the PCAC properties of T2Cs in the Bulge and the Magellanic Clouds for the very first time, to the best of our knowledge using the best available data and pulsation codes and compare with results for Cepheids and RR Lyraes. Hence this project aims to find direct observational evidence supporting the HIF-stellar photosphere interaction in the outer envelopes of variable stars and to probe the PC relation across a broad spectrum of classical pulsating stars in different evolutionary stages.

The structure of this paper is as follows: The theoretical motivation of this project is discussed in Section 2 while Section 3 describes the observational data used in this analysis and the Fourier decomposition technique. The extinction-corrected period-colour and amplitude-colour relations are briefly discussed in Section 4. We study the distance between the HIF and the stellar photosphere of RR Lyrae, BL Her and classical Cepheid models computed using MESA in Section 5. Finally, we summarise the results of this study in Section 6.

## 2 THEORETICAL FRAMEWORK

Kanbur (1995) found that the HIF was further out in the mass distribution in RR Lyrae stars as compared to classical Cepheids, i.e., the HIF is closer to the surface of the star with a higher effective temperature. In fact, Kanbur (1995) noted that the HIF lies further in the mass distribution as  $L/M$  increases and as  $T_{\text{eff}}$  decreases. While this result may be expected because Cepheids are cooler than RR Lyraes, it is nevertheless instructive and important to be able to demonstrate it both computationally and theoretically. To physically justify this statement, let  $\tau$  be the optical depth in terms of the Rosseland mean opacity. Then the temperature  $T$  in the stellar envelope can be approximated by

$$T^4(\tau) = \frac{3}{4} T_{\text{eff}}^4 [\tau + q(\tau)] \quad (1)$$

where  $T_{\text{eff}}$  is the effective temperature and  $q(\tau)$  is the Hopf function, a monotonically increasing function of  $\tau$  (e.g., Hopf 1930). We may consider  $T_{\text{eff}}$  to be constant at  $\sim 10000\text{K}$  at the base of the HIF. Since  $q(\tau)$  increases monotonically with  $\tau$ , the opacity of the HIF increases with decreasing effective temperature. Therefore, the HIF lies farther from the surface when the star is cooler.

To investigate and contextualize this within the stellar evolution theory, we used MESA to calculate the evolution of a star with an initial mass of  $0.83 M_{\odot}$  and initial composition of  $Y = 0.25$ ,  $Z = 0.001$  and study the relative location of the HIF and

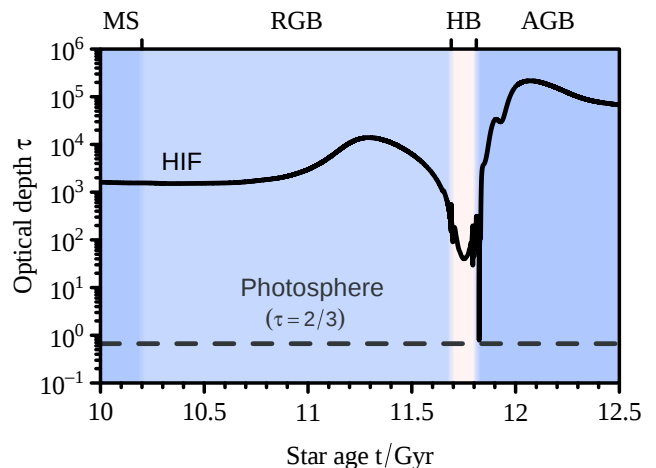


**Figure 1.** The location of the hydrogen ionization front compared to the photosphere as a function of stellar age for a low-mass star ( $M \approx 0.632 M_{\odot}$ ).

the stellar photosphere as it moves off the horizontal branch. We used the Grevesse & Sauval (1998, GS98) mixture for heavy-mass elements, nuclear reaction rates from the *Nuclear Astrophysics Compilation of Reaction Rates* (NACRE, Angulo et al. 1999), and the *Opacity Project at Livermore* (OPAL) equation of state and type-two opacities (Iglesias & Rogers 1996; Rogers & Nayfonov 2002). We treated convection using Böhm-Vitense (1958) mixing-length theory with a solar-calibrated mixing length ( $\alpha_{\text{MLT}} \approx 1.84$ ). We calculated mass loss using Reimers’ prescription with a mass loss rate of  $\eta = 0.5$  (Reimers 1975; Fadeyev 2019). We tracked the evolution from the pre-main sequence through the main sequence (MS), up the red giant branch (RGB), past the helium flash, onto the horizontal branch (HB), and finally onto the asymptotic giant branch (AGB).

Fig. 1 displays the location of the HIF compared to the photosphere as a function of stellar age. We note that this relative location or distance varies considerably during the evolutionary track. During the HB phase of evolution, the HIF is located near to the stellar photosphere (Kanbur 1995). After the exhaustion of helium in the core, when the star moves off the HB, it moves to brighter luminosities and cooler temperatures. That is, its  $L/M$  ratio increases and its  $T_{\text{eff}}$  decreases. Consequently, the HIF moves deeper into the mass distribution of the star. Figs. 1, 2 and 3 display these arguments. Fig. 1 presents the relative location of the photosphere and HIF at various stages during the life of a  $0.632M_{\odot}$  star. The star has an initial mass of  $0.83M_{\odot}$  and only reaches this low mass at the advanced stages of evolution. After the HB phase we see clearly that the HIF moves further away from the photosphere. Figs. 2 and 3 display this in greater detail. The left panel of Fig. 2 presents the location of this star on the HB whilst the right panel displays its outer envelope structure - specifically its temperature, opacity and ionized hydrogen structure. Fig. 3 is the same but for a star on the AGB. We clearly see that as the star moves to the AGB, its HIF moves further into the mass distribution.

## 3 DATA AND METHODS

In order to confirm these proposed HIF-photosphere interactions, we now obtain the PCAC relations from observations for stars at

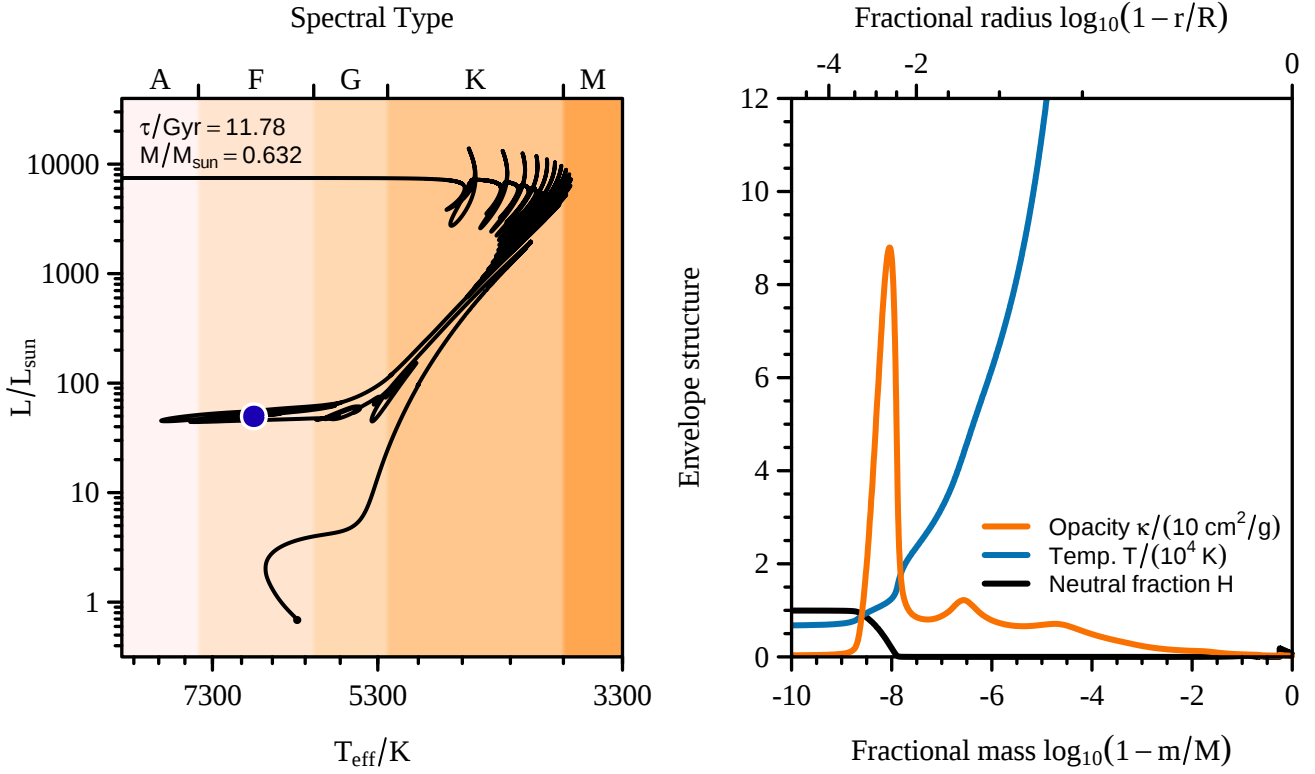


**Figure 2.** *Left panel:* Hertzprung-Russell diagram showing the theoretical evolution of a low-mass star with  $M_{\text{init}} = 0.83 M_{\odot}$ . The blue dot shows the position of an RR Lyrae-type star on the horizontal branch. The current mass and age of the model are indicated in the legend. *Right panel:* The thermodynamic envelope structure for the model indicated in the left panel. The hydrogen ionization front of an RR Lyrae star at equilibrium is located near to the stellar photosphere.

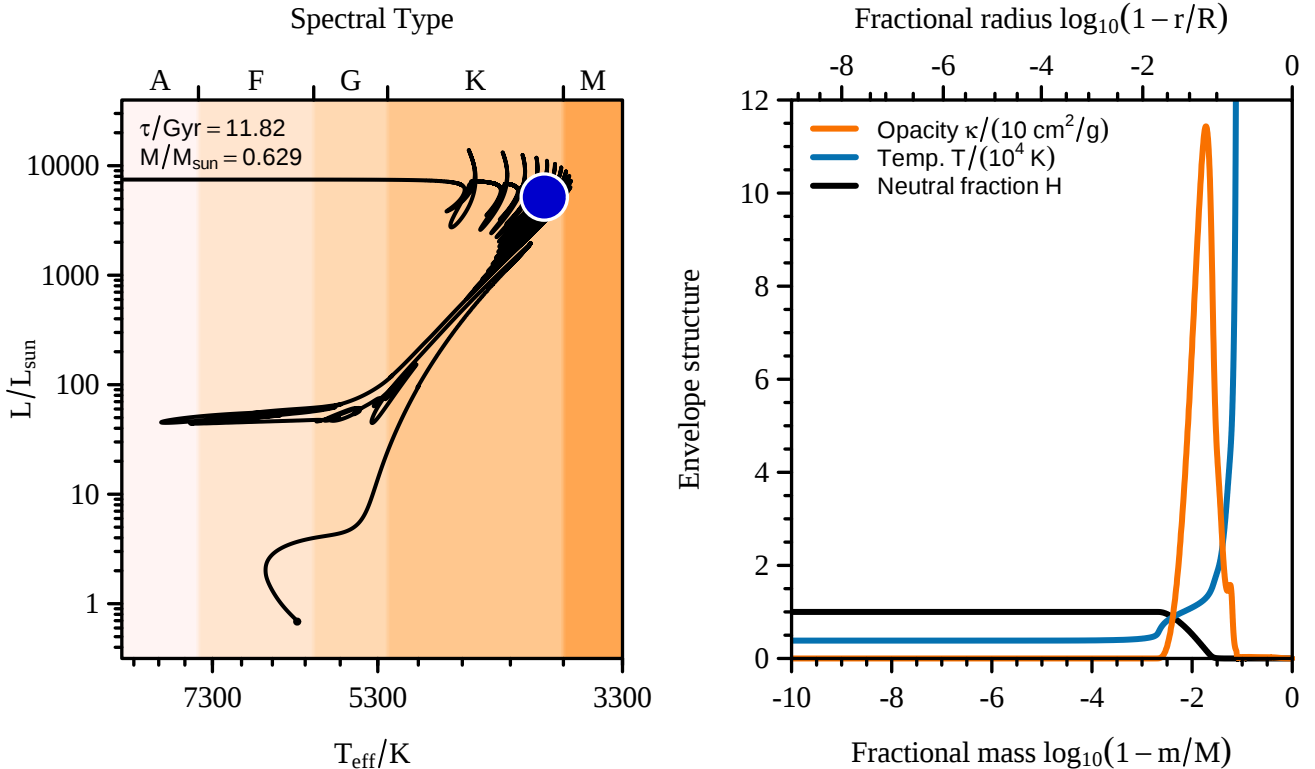


**Figure 3.** The same as Figure 2, but at a later stage of evolution; now on the asymptotic giant branch. The hydrogen ionization front for an AGB star at equilibrium is located deeper into the stellar interior.

**Table 1.** The observed light curve data used in the present analysis with the number of stars available in each dataset.  $N_{\text{Cep}}$  refers to the number of fundamental mode classical Cepheids while  $N_{\text{T2C}}$  is the total number of type II Cepheids available in each band for each source.

Source	Band	$N_{\text{Cep}}$	Reference	$N_{\text{T2C}}$	$N_{\text{BL Her}}$	$N_{\text{W Vir}}$	$N_{\text{pW Vir}}$	$N_{\text{RV Tau}}$	Reference
Bulge (OGLE-IV)	V	5	Soszyński et al. (2017)	517	221	193	18	85	Soszyński et al. (2017)
	I	30		873	372	336	30	135	
LMC (OGLE-IV)	V	2027	Soszyński et al. (2015)	243	76	92	24	51	Soszyński et al. (2018)
	I	2404		253	80	96	25	52	
SMC (OGLE-IV)	V	2422	Soszyński et al. (2015)	52	20	15	7	10	Soszyński et al. (2018)
	I	2687		52	20	15	7	10	

various stages of stellar evolution. The optical ( $VI$ ) light curves of the classical Cepheids and T2Cs in the Galactic bulge are taken from the OGLE-IV catalog (Soszyński et al. 2017) while those in Large Magellanic Cloud (LMC) and Small Magellanic Cloud (SMC) are taken from Soszyński et al. (2015) for classical Cepheids and from Soszyński et al. (2018) for T2Cs. The classification for the different subclasses of T2Cs is as provided by OGLE-IV. For our analysis, we choose the stars with well-sampled light curves having more than 30 data points in both  $V$  and  $I$  bands. The number of stars available for classical Cepheids and T2Cs is summarized in Table 1.

The photometric light curve data are fitted with the Fourier sine series (see example, Deb & Singh 2009; Bhardwaj et al. 2015; Das et al. 2018):

$$m = m_0 + \sum_{k=1}^N A_k \sin(2\pi kx + \phi_k), \quad (2)$$

where the phase  $x$  is calculated as:

$$x = \frac{(t - t_0)}{P} - \text{int}\left(\frac{t - t_0}{P}\right), \quad (3)$$

where  $t_0$  is the epoch of maximum brightness and  $P$  is the pulsation period. The order of the fit,  $N$  is obtained using the Bart's criteria (Bart 1982) by varying it from 4 to 8. From the Fourier-fitted light curves, we obtain colour at maximum, minimum and mean light as:

$$\begin{aligned} (V - I)_{\text{max}} &= V_{\text{max}} - I_{\text{phmax}}, \\ (V - I)_{\text{min}} &= V_{\text{min}} - I_{\text{phmin}}, \\ (V - I)_{\text{mean}} &= V_{\text{mean}} - I_{\text{mean}}, \end{aligned} \quad (4)$$

where  $I_{\text{phmax}}$  and  $I_{\text{phmin}}$  correspond to the  $I$ -magnitude at the same phase as that of  $V_{\text{max}}$  and  $V_{\text{min}}$ , respectively. The amplitude in  $V$  is simply defined as the difference between the maximum and minimum of the magnitude in the  $V$ -band.

To correct for extinction in the classical Cepheids and T2Cs in the LMC and SMC, we obtain their colour excess  $E(V - I)$  values using the reddening maps of Haschke et al. (2011) and convert to their  $E(B - V)$  values using  $E(V - I) = 1.38E(B - V)$  (Tammann et al. 2003). The extinction values are found by adopting the reddening law of Cardelli et al. (1989):  $A_V = 3.32E(B - V)$ ;  $A_I = 1.94E(B - V)$  (Schlegel et al. 1998).

For the T2Cs in the Galactic bulge, we first use the extinction maps of Gonzalez et al. (2012) and adopt the standard reddening law from Cardelli et al. (1989) ( $\frac{A_{K_s}}{A_V} = 0.114$ ;  $\frac{A_I}{A_V} = 0.479$ ). Given the non-standard nature of the reddening law towards the central Galactic bulge (Popowski 2000; Udalski 2003; Nishiyama et al. 2009; Nataf et al. 2013; Matsunaga et al. 2013), we also use the

extinction calculator provided by Nataf et al. (2013) to obtain the colour excess  $E(V - I)$  and extinction  $A_I$ . This calculator primarily assumes the  $E(J - K_s)$  measurements of Gonzalez et al. (2012). The  $A_V$  values are then estimated by using  $E(V - I) = A_V - A_I$ . We only use the first method of extinction correction for the classical Cepheids in the Galactic bulge.

These extinction corrections are applied to the magnitudes and colours at minimum, mean, and maximum light during the pulsation cycle. We fit linear-regression models to extinction corrected PC and AC relations for different classes of pulsating stars. Throughout this paper, we employ an iterative  $3\sigma$  outlier clipping during the regression analysis and points beyond this threshold are considered outliers.

## 4 ANALYSIS AND RESULTS

### 4.1 The statistical tests

#### 4.1.1 The $F$ -test

Earlier studies by Kanbur & Ngeow (2004) and Bhardwaj et al. (2014) showed a break in the PC relations for fundamental mode classical Cepheids in LMC and SMC at a period of 10 days at both minimum and maximum light. To test for any possible break in the PC relations for OGLE-IV classical Cepheids in the Magellanic Cloud, we use the  $F$ -test, which has been well-described in Kanbur & Ngeow (2004) and Bhardwaj et al. (2014). We briefly outline the method here: a single regression line may fit the data over the entire period range under the null hypothesis while two separate regression lines are required to fit the data having periods shorter/longer than 10 days under the alternate hypothesis, where we are testing for a break in the PC relation at a period of 10 days. The reduced model under the null hypothesis may then be written as:

$$(V - I)_{\text{max/min}} = a + b \log(P), \quad (5)$$

and the full model under the alternate hypothesis is:

$$\begin{aligned} (V - I)_{\text{max/min}} &= a_S + b_S \log(P); \text{ where } P < 10 \text{ days} \\ &= a_L + b_L \log(P); \text{ where } P \geq 10 \text{ days,} \end{aligned} \quad (6)$$

where  $(V - I)_{\text{max/min}}$  is colour at maximum or minimum light.

The  $F$  statistic is defined as follows (see example, Kanbur & Ngeow 2004; Bhardwaj et al. 2014):

$$F = \frac{RSS_R - RSS_F / [(n - 2) - (n - 4)]}{RSS_F / (n - 4)}, \quad (7)$$

where  $RSS_R$ ,  $RSS_F$  are the residual sums of squares in the reduced



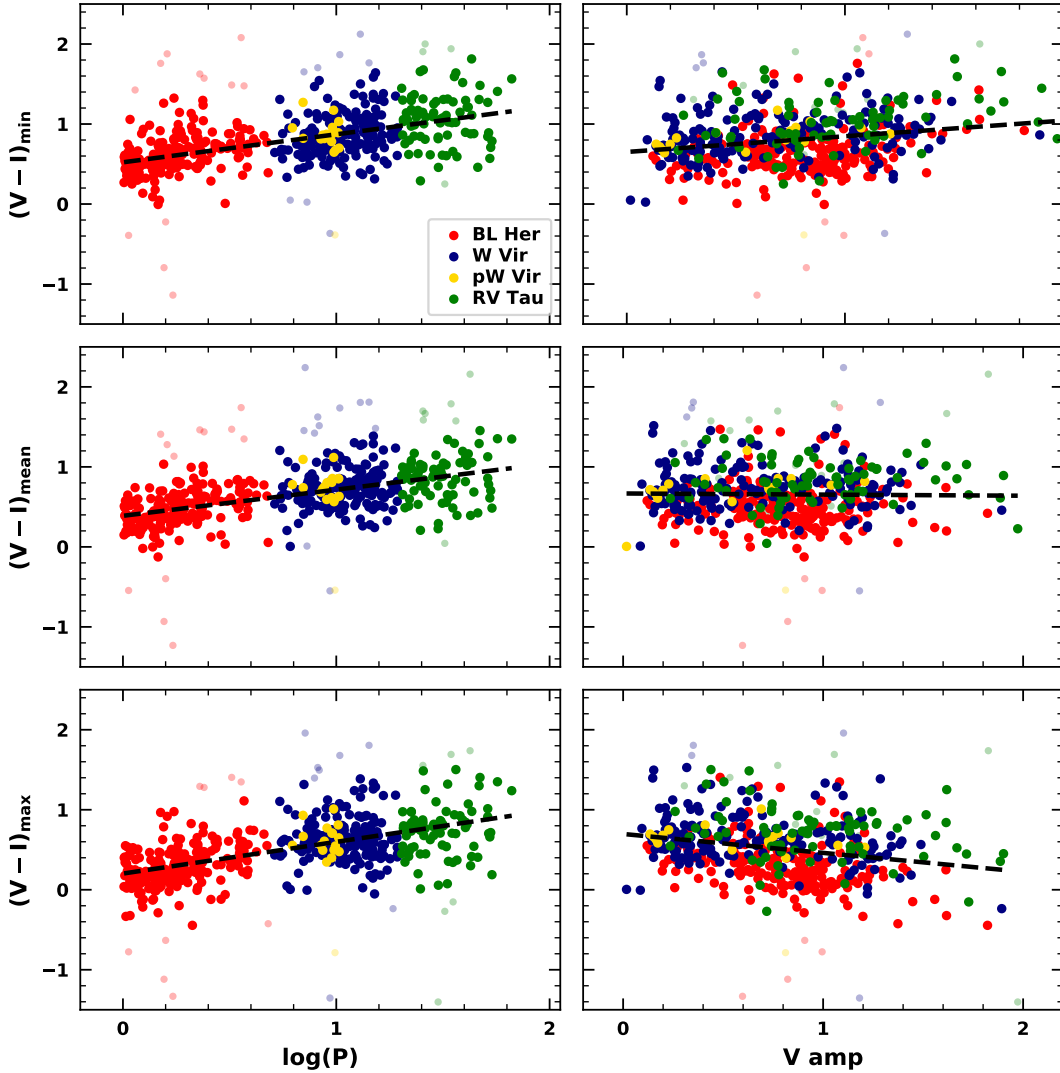


**Figure 4.** PC and AC relations for T2Cs in the Bulge from OGLE-IV at minimum, mean and maximum light. The different sub-classes are shown in different colours. However, the dashed line is the best fit linear regression for T2Cs as a whole with the different sub-classes combined, after recursively removing the  $3\sigma$  outliers (depicted in smaller, shaded symbols). The PC and AC relations obtained for the sub-classes separately may be found in Table 2.

model and the full model, respectively and  $n$  is the total number of stars in the entire dataset. The statistical significance of the variation in slopes at periods shorter/longer than 10 days may be studied by comparing the observed value of the  $F$  statistic with the critical value,  $F_C = F_{2,n-4}$  at 95% confidence level. An  $F$  statistic greater than the critical value or the probability of the observed value of the  $F$  statistic,  $P(F) < 0.05$  would mean the rejection of the null hypothesis, thereby confirming the presence of a break in the PC relation at 10 days.

#### 4.1.2 The $t$ -test

We use the standard  $t$ -test to statistically check the equivalence of PC slopes of different types of pulsating variable stars. We briefly outline the method here; detailed description may be found in Ngeow et al. (2015). The  $T$  statistic to compare slopes,  $\hat{W}$  of two linear regressions with sample sizes,  $n$  and  $m$ , respectively is de-

finied as:

$$T = \frac{\hat{W}_n - \hat{W}_m}{\sqrt{\text{Var}(\hat{W}_n) + \text{Var}(\hat{W}_m)}}, \quad (8)$$

where  $\text{Var}(\hat{W})$  is the variance of the slope. The critical value under the two-tailed  $t$ -distribution is  $t_{\alpha/2,\nu}$ , where  $\alpha=0.05$  with 95% confidence limit and degrees of freedom,  $\nu = n + m - 4$ . The null hypothesis of equivalent PC slopes may be rejected if  $T > t_{\alpha/2,\nu}$  or the probability of the observed value of the  $T$  statistic,  $p < 0.05$ .

## 4.2 Period-colour and amplitude-colour relations

Simon et al. (1993) introduced the concept of PCAC at maximum and minimum light as a way to probe the radiation hydrodynamics of the outer envelope in Cepheids and were able to explain the flat and sloped PC relations for Galactic Cepheids at maximum and minimum light, respectively. This was extended in a series of pa-

**Table 2.** The slopes and intercepts for PC and AC relations for the four subclasses of the T2Cs in the Bulge, LMC and SMC. T2C refers to these subclasses combined together. The last column indicates whether the PC relation has a flat or a significant slope within  $3\sigma$  uncertainties.

Phase		PC			AC			Nature of PC slope
		Slope	Intercept	$\sigma$	Slope	Intercept	$\sigma$	
Bulge (OGLE-IV) using extinction law from <a href="#">Cardelli et al. (1989)</a>								
BL Her	min	0.516±0.073	0.475±0.023	0.173	0.216±0.053	0.45±0.045	0.219	Sloped
	mean	0.594±0.072	0.323±0.022	0.17	-0.057±0.05	0.518±0.043	0.208	Sloped
	max	0.636±0.088	0.122±0.028	0.21	-0.38±0.052	0.584±0.044	0.216	Sloped
W Vir	min	0.549±0.136	0.289±0.141	0.257	0.193±0.048	0.725±0.036	0.253	Sloped
	mean	0.276±0.122	0.444±0.126	0.228	0.032±0.047	0.72±0.036	0.247	Flat
	max	0.037±0.141	0.605±0.147	0.266	-0.172±0.05	0.751±0.038	0.266	Flat
pW Vir	min	-0.819±0.665	1.659±0.633	0.15	0.295±0.186	0.676±0.136	0.145	Flat
	mean	-0.487±0.671	1.232±0.639	0.151	0.089±0.196	0.707±0.144	0.153	Flat
	max	-0.23±0.769	0.85±0.732	0.173	-0.191±0.217	0.765±0.159	0.169	Flat
RV Tau	min	0.03±0.317	1.037±0.475	0.359	0.207±0.103	0.877±0.109	0.35	Flat
	mean	0.24±0.298	0.532±0.446	0.337	-0.084±0.099	0.972±0.105	0.337	Flat
	max	0.47±0.333	0.053±0.499	0.379	-0.322±0.103	1.071±0.108	0.334	Flat
T2C	min	0.35±0.023	0.522±0.021	0.244	0.196±0.038	0.651±0.032	0.307	Sloped
	mean	0.327±0.02	0.389±0.019	0.217	-0.014±0.036	0.668±0.031	0.293	Sloped
	max	0.396±0.024	0.202±0.022	0.26	-0.236±0.041	0.697±0.035	0.335	Sloped
Bulge (OGLE-IV) using extinction law from <a href="#">Nataf et al. (2013)</a>								
BL Her	min	0.389±0.058	0.58±0.018	0.107	0.063±0.042	0.639±0.034	0.13	Sloped
	mean	0.337±0.066	0.472±0.021	0.123	-0.097±0.04	0.63±0.033	0.123	Sloped
	max	0.374±0.102	0.298±0.032	0.194	-0.376±0.043	0.667±0.036	0.134	Sloped
W Vir	min	0.383±0.116	0.482±0.119	0.161	0.183±0.042	0.764±0.03	0.156	Sloped
	mean	0.043±0.108	0.736±0.112	0.153	0.021±0.041	0.768±0.029	0.153	Flat
	max	-0.151±0.12	0.848±0.124	0.169	-0.129±0.044	0.77±0.031	0.164	Flat
pW Vir	min	-0.37±0.765	1.263±0.733	0.139	0.313±0.19	0.709±0.129	0.122	Flat
	mean	-0.148±0.784	0.956±0.751	0.143	0.156±0.216	0.715±0.146	0.139	Flat
	max	0.121±0.894	0.581±0.857	0.163	-0.104±0.251	0.763±0.17	0.162	Flat
RV Tau	min	0.111±0.319	1.013±0.478	0.298	0.154±0.112	1.034±0.114	0.293	Flat
	mean	0.419±0.298	0.373±0.447	0.279	-0.136±0.107	1.126±0.108	0.28	Flat
	max	0.766±0.349	-0.267±0.524	0.33	-0.404±0.101	1.262±0.102	0.262	Flat
T2C	min	0.321±0.019	0.594±0.017	0.16	0.206±0.038	0.69±0.031	0.231	Sloped
	mean	0.316±0.017	0.472±0.015	0.14	0.031±0.037	0.697±0.03	0.227	Sloped
	max	0.36±0.023	0.31±0.021	0.194	-0.2±0.042	0.728±0.035	0.261	Sloped
LMC (OGLE-IV)								
BL Her	min	0.604±0.101	0.602±0.026	0.112	0.195±0.079	0.566±0.064	0.146	Sloped
	mean	0.585±0.062	0.453±0.016	0.067	0.009±0.069	0.571±0.056	0.127	Sloped
	max	0.44±0.104	0.293±0.027	0.121	-0.263±0.066	0.597±0.054	0.122	Sloped
W Vir	min	0.597±0.072	0.366±0.074	0.102	0.193±0.029	0.866±0.02	0.11	Sloped
	mean	0.203±0.059	0.651±0.061	0.082	0.018±0.023	0.85±0.016	0.09	Sloped
	max	-0.033±0.086	0.821±0.088	0.12	-0.137±0.032	0.855±0.022	0.122	Flat
pW Vir	min	0.468±0.26	0.235±0.233	0.195	0.322±0.118	0.49±0.07	0.18	Flat
	mean	0.528±0.209	0.116±0.187	0.157	0.157±0.113	0.504±0.067	0.172	Flat
	max	0.647±0.195	-0.091±0.174	0.146	-0.113±0.117	0.533±0.07	0.178	Sloped
RV Tau	min	-0.082±0.461	1.062±0.715	0.33	0.655±0.077	0.519±0.058	0.206	Flat
	mean	-0.088±0.291	0.918±0.451	0.208	0.32±0.04	0.566±0.031	0.105	Flat
	max	0.003±0.198	0.661±0.308	0.141	0.178±0.053	0.542±0.04	0.141	Flat
T2C	min	0.215±0.026	0.673±0.026	0.195	0.229±0.04	0.708±0.029	0.221	Sloped
	mean	0.209±0.02	0.555±0.02	0.151	0.037±0.033	0.706±0.024	0.185	Sloped
	max	0.269±0.024	0.372±0.024	0.182	-0.161±0.039	0.711±0.029	0.22	Sloped
SMC (OGLE-IV)								
BL Her	min	-0.251±0.339	0.759±0.088	0.175	0.434±0.115	0.445±0.076	0.129	Flat
	mean	-0.115±0.22	0.613±0.057	0.114	0.127±0.097	0.512±0.064	0.109	Flat
	max	-0.018±0.21	0.458±0.054	0.108	-0.12±0.092	0.525±0.06	0.103	Flat
W Vir	min	0.314±0.112	0.632±0.118	0.074	0.124±0.063	0.869±0.051	0.083	Flat
	mean	0.073±0.098	0.757±0.103	0.064	-0.032±0.049	0.854±0.04	0.065	Flat
	max	-0.169±0.189	0.89±0.199	0.125	-0.219±0.073	0.87±0.059	0.096	Flat
pW Vir	min	0.52±0.576	0.02±0.631	0.194	0.52±0.618	0.448±0.194	0.197	Flat
	mean	0.478±0.473	0.035±0.518	0.159	0.37±0.538	0.456±0.169	0.171	Flat
	max	0.484±0.408	-0.014±0.447	0.137	0.216±0.508	0.453±0.16	0.162	Flat
RV Tau	min	-0.366±0.507	1.492±0.773	0.137	0.199±0.14	0.799±0.108	0.123	Flat
	mean	-0.203±0.394	1.11±0.601	0.106	0.105±0.116	0.73±0.089	0.102	Flat
	max	0.198±0.475	0.38±0.725	0.128	-0.003±0.148	0.683±0.114	0.13	Flat
T2C	min	0.166±0.054	0.668±0.052	0.196	0.347±0.072	0.597±0.05	0.176	Sloped
	mean	0.16±0.04	0.563±0.039	0.145	0.156±0.064	0.601±0.045	0.158	Sloped
	max	0.177±0.04	0.435±0.039	0.147	-0.026±0.071	0.596±0.049	0.174	Sloped

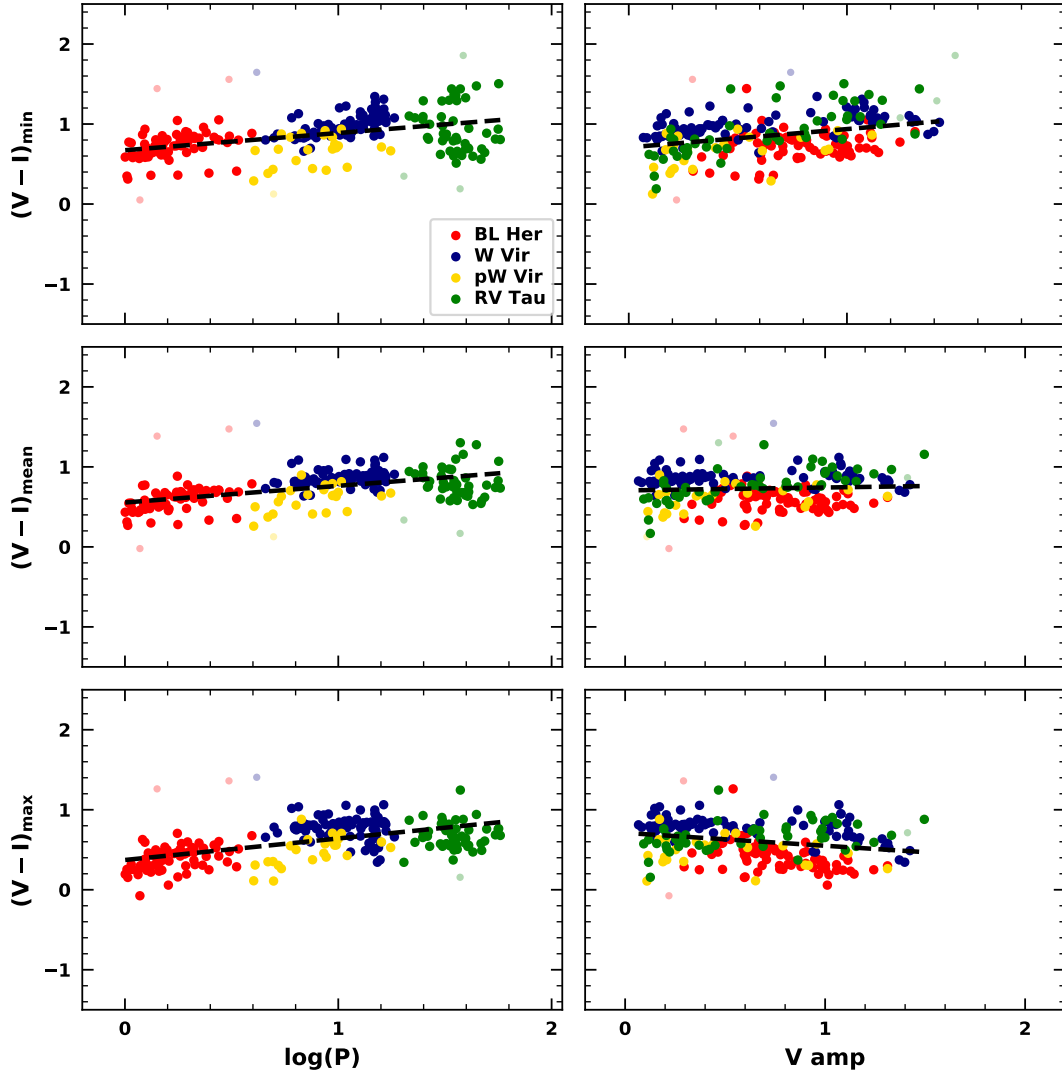


Figure 5. Same as Fig.4 but for LMC.

pers (Bhardwaj et al. 2014; Das et al. 2018, and references therein). Here we study PCAC relations for T2Cs and classical Cepheids using the latest available data.

#### 4.2.1 Type II Cepheids

The period-colour (PC) and amplitude-colour (AC) relations for the T2Cs in the Bulge, LMC and SMC from OGLE-IV are displayed in Figs. 4, 5 and 6, respectively at minimum, mean and maximum light. PC and AC relations are also obtained for different sub-classes of T2Cs separately. The summary of the PC and AC relations for different sub-classes as well as for all the T2Cs sample in the Bulge, LMC and SMC are listed in Table 2. First we discuss the PC relations of the W Vir stars. We observe a flat PC slope at maximum light for W Vir stars in the Bulge, LMC and SMC within  $3\sigma$  uncertainties. For W Vir stars, the  $PC_{\max}$  is flat but slightly negative ( $-0.033 \pm 0.086$  in the LMC and  $-0.169 \pm 0.189$  in the SMC). The flat  $PC_{\max}$  slope of W Vir stars is similar to that obtained for long period classical Cepheids ( $P > 10$ days) in Galaxy, LMC and

SMC (Bhardwaj et al. 2014). We note that the slope of PC relation at minimum light for W Vir stars is significantly greater than at maximum light. In fundamental mode classical Cepheids, the HIF and stellar photosphere are engaged at low densities only at maximum light leading to a flat PC relation. Apparent similarity in the behaviour of W Vir stars with long-period classical Cepheids in the PCAC plane suggests that HIF and stellar photosphere interactions are similar in these two classical pulsators as they also occupy the same region on the HR diagram.

In the PC relations of BL Her stars, we observe a significant, positive PC slope in the Bulge and the LMC and a flat (but negative) slope in the SMC at both minimum and maximum light. The sloped PC relations of BL Her stars in the Bulge and the LMC are similar to short period classical Cepheids ( $P < 10$ days). The flat but slightly negative  $PC_{\min}$  for BL Her stars in SMC ( $-0.251 \pm 0.339$ ) is similar to what Das et al. (2018) obtained for RR Lyrae stars in SMC at minimum light. We note here that the number of BL Her stars in SMC is very less ( $\sim 20$ ). The slopes of the PC relations for RV Tau stars in Bulge, LMC and SMC are flat within  $3\sigma$  un-



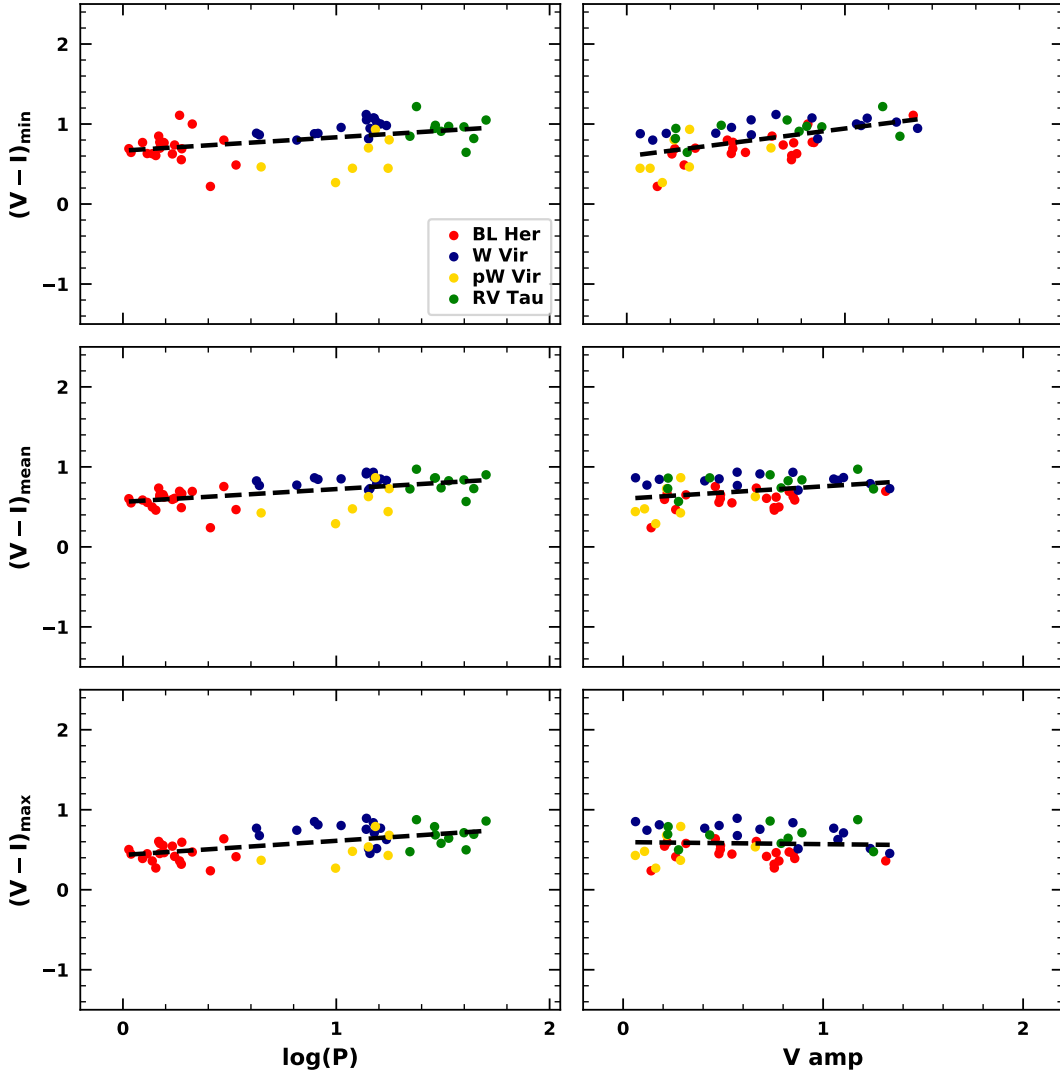


Figure 6. Same as Fig.4 but for SMC.

certainties at minimum and maximum light; however, there is high dispersion in all the cases.

#### 4.2.2 Classical Cepheids

The PC and AC relations for classical Cepheids in LMC and SMC from OGLE-IV are shown in Fig. 7 and summarised in Table 3. We have used the  $F$ -test to statistically identify any possible breaks in the PC and AC relations. As can be observed from Table 3, we find breaks in the PC as well as AC relations at a period of 10 days at both minimum and maximum light for classical Cepheids in LMC and SMC. The longer period classical Cepheids have a flat  $PC_{\max}$  within  $3\sigma$  uncertainties and a significantly sloped  $PC_{\min}$  relation for both LMC and SMC. Also, at maximum light, longer period classical Cepheids have a shallower  $PC_{\max}$  than their shorter period counterparts. This is similar to the results found in the earlier studies for classical Cepheids in LMC and SMC by Kanbur & Ngeow (2004) and Bhardwaj et al. (2014). We have excluded classical Cepheids in the Galactic bulge from any statistical test because of the avail-

ability of very few stars from the OGLE-IV dataset. We note that the PC relations at maximum/minimum show statistically different slopes between long and short period Cepheids and between the LMC and the SMC. In future work, these differences can be used to constrain extensive grids of Cepheid pulsation models.

#### 4.2.3 Comparison of Period-Colour relations

It is important to quantitatively compare the PC relations at maximum, mean and minimum light between the different classes of variable stars and different metallicity environments. Since previous work (Bhardwaj et al. 2014, and references therein) has suggested nonlinearities in PC relations, we investigate whether the data used in this paper show evidence of this. Nonlinearities in PC relations will be useful in constraining stellar pulsation and evolution models.

We summarize the results of the statistical  $t$ -test to compare PC slopes in the LMC and SMC across a broad spectrum of variable star types in Tables A1 and A2, respectively. The PC slopes of

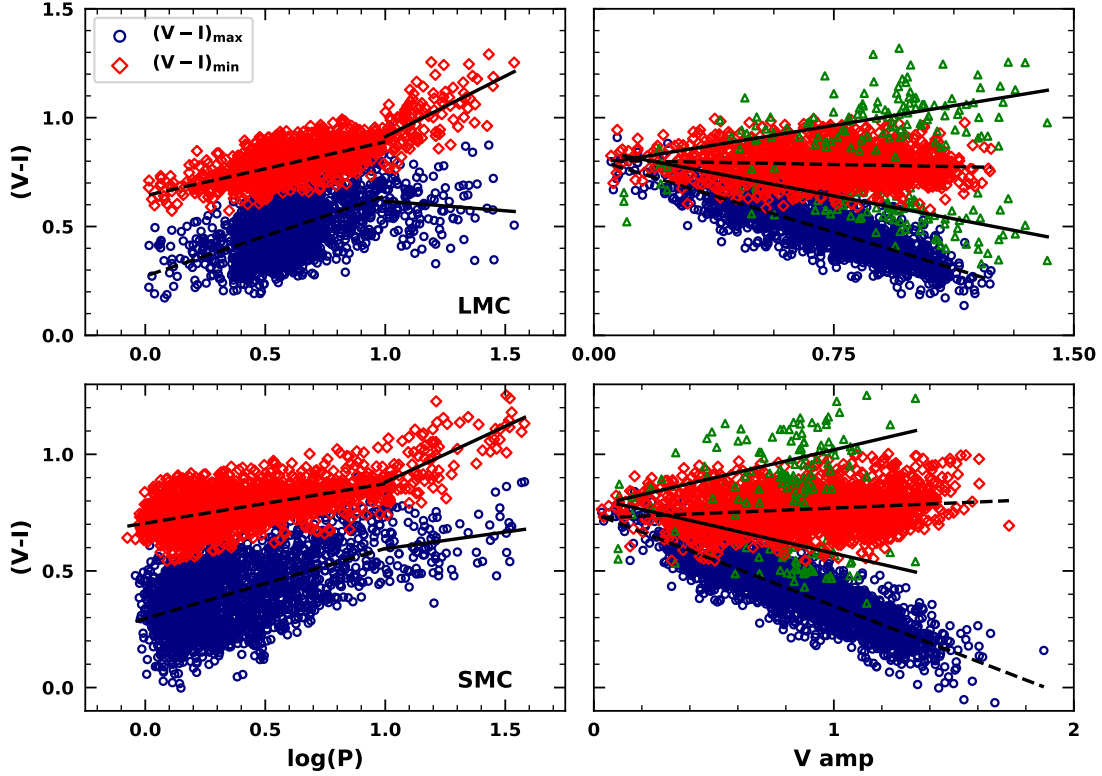


**Figure 7.** PC and AC relations for fundamental mode classical Cepheids from OGLE-IV at maximum and minimum light for LMC and SMC. The dashed/solid lines represent the best fit to shorter/longer period Cepheids separated at 10 days. Green triangles on the right represent the Cepheids having periods greater than 10 days at both maximum and minimum light.

**Table 3.** Results of F test on PC and AC relations for fundamental mode Cepheids from OGLE-IV to determine possible nonlinearities at 10 days. The bold-face entries indicate existence of break in PC/AC at 10 days.

Phase		$b_{all}$	$a_{all}$	$b_S$	$a_S$	$b_L$	$a_L$	F	P(F)
LMC									
PC	max	0.294±0.011	0.312±0.007	0.369±0.015	0.272±0.009	-0.088±0.087	0.705±0.101	28.448	<b>0.000</b>
	mean	0.246±0.006	0.539±0.004	0.228±0.008	0.549±0.005	0.419±0.062	0.358±0.072	2.772	0.063
	min	0.294±0.006	0.618±0.004	0.247±0.008	0.642±0.004	0.556±0.067	0.356±0.078	11.202	<b>0.000</b>
AC	max	-0.421±0.008	0.797±0.006	-0.447±0.007	0.81±0.006	-0.281±0.032	0.851±0.03	143.275	<b>0.000</b>
	mean	-0.132±0.007	0.784±0.006	-0.148±0.007	0.791±0.005	0.109±0.032	0.743±0.029	145.555	<b>0.000</b>
	min	-0.002±0.008	0.793±0.007	-0.026±0.008	0.804±0.006	0.242±0.036	0.783±0.033	180.097	<b>0.000</b>
SMC									
PC	max	0.284±0.009	0.301±0.004	0.301±0.011	0.296±0.005	0.143±0.07	0.452±0.085	7.141	<b>0.001</b>
	mean	0.205±0.004	0.569±0.002	0.188±0.005	0.573±0.002	0.432±0.055	0.316±0.066	5.093	<b>0.006</b>
	min	0.197±0.005	0.696±0.002	0.17±0.006	0.705±0.002	0.478±0.056	0.402±0.068	13.24	<b>0.000</b>
AC	max	-0.398±0.005	0.751±0.005	-0.396±0.005	0.746±0.005	-0.236±0.044	0.811±0.036	218.073	<b>0.000</b>
	mean	-0.113±0.004	0.74±0.004	-0.111±0.004	0.736±0.004	0.082±0.049	0.768±0.04	227.841	<b>0.000</b>
	min	0.042±0.006	0.731±0.005	0.043±0.005	0.726±0.005	0.241±0.05	0.778±0.041	193.507	<b>0.000</b>

RRab stars in LMC and SMC using OGLE-IV data have been taken from our recent work (Das et al. 2018). We discuss the results from this comparison below:-

(i) Slopes of the PC relation for W Vir stars are equivalent with those for the longer-period classical Cepheids at both minimum and maximum light for LMC but only at minimum light for SMC.

(ii) The  $PC_{min}$  slopes for BL Her stars and RRab stars in SMC are statistically similar.

(iii) BL Her stars have statistically similar PC slopes with those from longer period classical Cepheids in LMC at minimum light and with those in SMC at maximum light.

(iv) In SMC, BL Her stars have PC slopes equivalent with those

from W Vir stars at both minimum and maximum light while in LMC, they are statistically similar only at minimum light.

(v) BL Her stars have PC slopes equivalent with those from shorter period classical Cepheids at both minimum and maximum light in SMC but only at maximum light for those in LMC.

(vi) For both LMC and SMC, PC slopes from W Vir stars and RRab stars exhibit different behaviour at minimum and maximum light.

(vii) As expected, RRab stars and classical Cepheids never have similar PC slopes; this is because of the existence of flat  $PC_{\min}$  for RRab with a significantly sloped  $PC_{\max}$  and flat  $PC_{\max}$  for classical Cepheids with a significant slope in  $PC_{\min}$ .

The central result from these tables is the following: RRab stars have a flat or shallow slope at minimum light and a statistically significant larger slope at maximum light. BL Her stars have a much smaller difference between the PC slopes at maximum/minimum light than RRab stars, similar to short-period classical Cepheids. WVir stars, in contrast, have statistically significant flat or shallow (perhaps negative) slopes at maximum light and a statistically significant non-zero slope at minimum light - a situation that is similar to that of long-period classical Cepheids. There may be further real differences between different galaxies, but for this paper we concentrate on this broad conclusion and seek to explain this in terms of the detailed physics of the outer envelope and how this changes as a result of stellar evolution.

We also see that the PCAC analysis of OGLE-IV data displayed in Fig. 7 and quantified in Table 3 portray very clearly a sharp break in the PCAC relations at a period close to 10 days. This is consistent with previous work by Bhardwaj et al. (2014) using OGLE-III data. The interpretation of this break in the PC relation arises from arguments given in Kanbur et al. (2007); Bhardwaj et al. (2014), and references therein regarding the interaction of the HIF and stellar photosphere. For periods shorter than about 10 days, the HIF and stellar photosphere are engaged at high temperatures and hence the temperature of the photosphere is the temperature at which hydrogen ionizes. This is in a regime where Saha ionization equilibrium is sensitive to temperature and density and hence, sensitive to global stellar parameters. Since colour is a measure of the temperature of the photosphere and period is dependent on global stellar parameters through the period-mean density theorem, we would expect a non-zero slope for the PC relation. However, as the  $L/M$  ratio goes up and the temperature goes down, the period increases and the HIF and photosphere become disengaged at many phases, except around maximum light when the HIF is at its furthest point in the mass distribution. This engagement at maximum light at lower temperatures and densities implies that the temperature of the stellar photosphere is again the temperature at which hydrogen ionizes but this time the temperature at which hydrogen ionizes is somewhat independent of global stellar parameters and hence we have a flatter PC slope for these long period Cepheids. The AC part of PCAC arise from arguments first presented in Simon et al. (1993): changes in PC relations will be reflected in AC relations and this is what we find. OGLE-IV PCAC results for RR Lyrae stars are presented in Das et al. (2018) and again are consistent with the above ideas. Hence it is important to see how the latest available data for T2Cs in different metallicity environments compare to results for Cepheids and RR Lyraes.

## 5 HIF-STELLAR PHOTOSPHERE INTERACTION - THE THEORETICAL APPROACH

Several aspects of our theoretical approach have been outlined in the introduction and earlier sections and in earlier papers (Simon et al. 1993; Kanbur 1995; Kanbur & Phillips 1996; Kanbur et al. 2004; Kanbur & Ngeow 2006; Kanbur et al. 2007). In summary, the properties of mean light PC relations are determined by the properties of PC relations at different phases during a pulsation cycle and at maximum and minimum light, these are determined by the interaction of the stellar photosphere and the HIF.

In an effort to understand the interaction of the HIF and the stellar photosphere during the pulsation cycle, we theoretically study the HIF-stellar photosphere distance (see Kanbur et al. 2004) at minimum and maximum light using the radial stellar pulsation code in MESA. We use MESA r-11701 (Paxton et al. 2019) to compute RR Lyrae, BL Her and classical Cepheid models, the parameters of which are listed in Table 4. We chose this pulsation code because it is a state-of-the-art pulsation code that is open source. Further it allows some flexibility in treatments of turbulent convection and opens up the possibility of using future detailed studies to constrain theories of turbulent convection in classical Cepheids and RR Lyraes. Here we show that in terms of light curves, it matches observations well. In common with many other pulsation codes (Marconi et al. 2015) it uses the diffusion approximation to model radiative transfer, though future plans include more sophisticated treatments of radiative transfer.

The input parameters for these models ( $Z$ ,  $X$ ,  $M/M_{\odot}$ ,  $L/L_{\odot}$  and  $T_{\text{eff}}$ ) have been taken from literature (see e.g. Marconi et al. 2015 for RR Lyraes, Marconi & Di Criscienzo 2007 for BL Her models and Table 1 of Kanbur et al. 2004 for classical Cepheids). We may choose to use any of the four sets of convection parameters as outlined in Table 4 of Paxton et al. (2019). Set A corresponds to the simplest convection model, set B adds radiative cooling, set C adds turbulent pressure and turbulent flux, and set D includes these effects simultaneously. In the present work, we choose to use the simplest (Set A) and the most complex (Set D) convection models for the same input parameters. A study of the effect of different sets of convection parameters on the light curve structures of the models is planned for the future. For our analysis, we proceed with only those models that have full-amplitude stable pulsations in the fundamental mode. Fourier analysis of these models shows considerably good match between the models and observations in the Galactic bulge, LMC and SMC for OGLE-IV RR Lyraes, BL Her stars and classical Cepheids with respect to their Fourier parameters and thus, their light curve structures.

### 5.1 Theoretical period-temperature and period-colour relations at maximum and minimum light

The variation of temperature with period for the computed models at minimum and maximum light is displayed in Fig. 8 and tabulated in Table 5. We find a relatively well-defined period-temperature relation at minimum light across different types of pulsating variable stars considered. However, there is a higher dispersion in the period-temperature relation for the same models at maximum light. Considering RR Lyrae models, while the temperature range between the reddest and the bluest models at minimum light is  $\sim 500\text{K}$ , it is as high as  $\sim 2000\text{K}$  at maximum light. Also note that if we were to expand the period scale, we would find the period-temperature relation for RRab stars at minimum light to be relatively shallow, consistent with observations. From Table 5 we find

**Table 4.** A summary of the RR Lyrae, BL Her and classical Cepheid models computed with MESA for the present analysis with a unique combination of ( $Z$ ,  $X$ ,  $M/M_{\odot}$ ,  $L/L_{\odot}$  and  $T_{\text{eff}}$  (K)).  $P_A$  and  $P_D$  indicate period in days using convection sets A and D, respectively. All the models presented here are fundamental mode pulsators. The entries marked with “-” are those that did not have full-amplitude stable pulsations in the fundamental mode.

$Z$	$X$	$\frac{M}{M_{\odot}}$	$\frac{L}{L_{\odot}}$	$T_{\text{eff}}$ (K)	$P_A$	$P_D$
RR Lyrae models						
0.001	0.754	0.64	46.77	6800	0.49833	0.36771
0.001	0.754	0.64	46.77	6300	0.65492	0.65561
0.001	0.754	0.58	74.13	6900	0.73759	–
0.001	0.754	0.58	74.13	6700	0.82012	0.60037
0.001	0.754	0.64	97.72	6600	1.02266	1.02203
0.001	0.754	0.64	97.72	6700	0.96767	–
0.02	0.71	0.54	30.90	6800	0.41861	0.29709
0.02	0.71	0.54	30.90	6700	0.44036	0.31198
0.02	0.71	0.54	30.90	6500	0.48886	0.48887
0.004	0.746	0.59	40.74	6900	0.45505	0.33229
0.0006	0.7544	0.67	48.98	6800	0.49924	0.37066
0.008	0.736	0.56	39.81	6900	0.46738	0.33825
0.001	0.754	0.64	46.77	6200	0.69655	0.69808
0.001	0.754	0.64	46.77	6400	0.6178	0.61794
0.001	0.754	0.64	46.77	6500	0.58415	0.58414
0.001	0.754	0.64	46.77	6600	0.55327	0.55312
0.001	0.754	0.64	46.77	6700	0.52477	0.36918
BL Her models						
0.0001	0.7599	0.6	89.12	6300	1.16531	1.1663
0.001	0.759	0.55	64.56	6250	0.98055	0.98211
0.001	0.759	0.65	81.28	6200	1.09424	1.09615
0.001	0.759	0.65	64.56	6200	0.90085	0.90257
0.001	0.759	0.65	81.28	6600	0.8668	0.63547
0.001	0.759	0.65	102.33	6200	1.33299	1.33625
0.004	0.756	0.55	102.33	5950	1.81067	1.82324
0.0001	0.7599	0.65	128.82	5750	2.20416	2.25865
0.0001	0.7599	0.6	141.25	5750	2.52525	2.58125
0.0004	0.75	0.6	150	5780	2.60992	2.65789
0.0004	0.75	0.6	175	5780	2.98105	3.03453
0.0004	0.75	0.6	300	5780	4.81726	4.88523
0.004	0.756	0.55	64.56	5950	1.21133	1.22078
0.004	0.756	0.55	64.56	6750	0.75042	0.54628
0.004	0.756	0.55	81.28	5850	1.61118*	1.61118
0.004	0.756	0.55	81.28	6650	0.9599	0.95901
0.004	0.756	0.55	102.33	5650	2.24159	2.31228
0.0001	0.7599	0.65	128.82	6225	1.58928	1.589
0.0001	0.7599	0.6	141.25	5600	2.85031	2.99971
Classical Cepheid models						
0.02	0.7	5.1	3006.08	5396	10.32019	10.32818
0.02	0.7	7.7	4965.92	5332	12.46112	–
0.02	0.7	6.3	6456.54	5390	17.69231	17.68952
0.02	0.7	9.45	9862.79	5265	20.88859	–
0.004	0.746	6.8	8709.64	5200	24.49454	24.84936
0.004	0.746	6.8	8709.64	5000	28.59717	29.59406
0.004	0.746	6.6	7762.47	4900	28.51875	30.12038
0.004	0.746	6.6	8709.64	4900	31.74634	33.49494
0.004	0.746	6.8	8709.64	4800	–	36.41581
0.02	0.7	10	34197.94	5100	78.4023	–
0.02	0.7	9	23388.37	5100	57.05626	58.18299
0.008	0.736	4.5	1258.92	5960	3.59225	2.55345
0.008	0.736	6	3981.07	5625	9.8025	9.79768
0.008	0.736	8	10000	5370	21.88827	21.9776
0.008	0.736	10	19952.62	5310	36.90233	37.16359
0.008	0.742	5.6	1995.26	5900	4.75799	–
0.004	0.746	5.4	2238.72	5900	5.2892	–
0.004	0.746	5.4	2238.72	5800	5.62694	4.04213
0.008	0.742	5.6	1995.26	5500	6.12775	6.1435
0.008	0.742	5.8	2238.72	5500	6.60143	6.61745
0.004	0.746	6.2	3548.13	5900	7.14526	5.09709
0.008	0.742	6.2	2818.38	5400	8.22863	8.26111

\*Period is obtained from Set D.

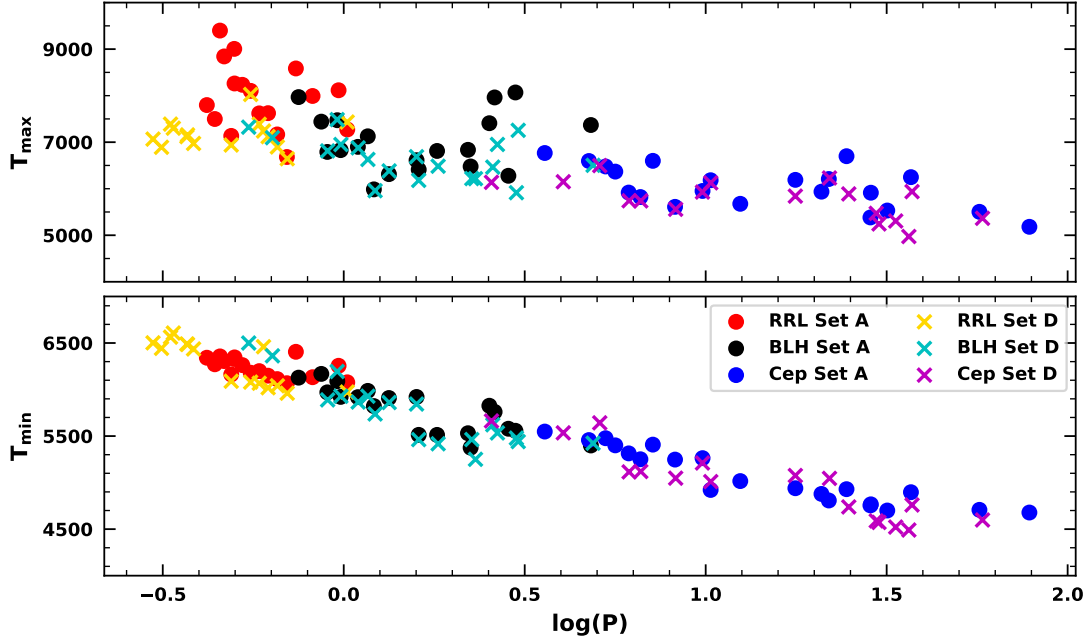


**Figure 8.** The variation of temperature at maximum and minimum light with period for the computed models using convection sets A and D.

**Table 5.** The slopes and intercepts for period-temperature relations of the mathematical form  $\log(T) = a \log(P) + b$  for RR Lyrae, BL Her and Cepheid models at minimum and maximum light.

Model	Minimum light			Maximum light		
Convection set A						
	$a$	$b$	$\sigma$	$a$	$b$	$\sigma$
RRL	$-0.032 \pm 0.014$	$3.787 \pm 0.004$	0.006	$-0.1 \pm 0.082$	$3.877 \pm 0.021$	0.037
BLH	$-0.07 \pm 0.012$	$3.776 \pm 0.003$	0.011	$0.012 \pm 0.041$	$3.841 \pm 0.012$	0.036
Cep	$-0.062 \pm 0.005$	$3.775 \pm 0.006$	0.008	$-0.052 \pm 0.016$	$3.839 \pm 0.019$	0.026
Convection set D						
	$a$	$b$	$\sigma$	$a$	$b$	$\sigma$
RRL	$-0.092 \pm 0.016$	$3.768 \pm 0.006$	0.009	$0.013 \pm 0.034$	$3.859 \pm 0.012$	0.018
BLH	$-0.089 \pm 0.012$	$3.776 \pm 0.004$	0.012	$-0.054 \pm 0.026$	$3.832 \pm 0.008$	0.026
Cep	$-0.076 \pm 0.008$	$3.784 \pm 0.01$	0.013	$-0.048 \pm 0.016$	$3.816 \pm 0.019$	0.023

that a flat (or flatter) period-temperature relation at maximum light within  $3\sigma$  uncertainties exists for RR Lyraes, BL Her and Cepheid models using both sets of convection parameters while RRL models also have a flat period-temperature relation at minimum light using the convection set A.

The PC and AC relations from the computed models are summarised in Table 6. The PC slopes from RR Lyrae and Cepheid models do not compare well with observations which show flat  $PC_{\min}$  for RRab stars and flat  $PC_{\max}$  for long-period classical Cepheids. However, we point here that the reason may be due to the fewer number of models used. A future study would involve computing a fine grid of models to rigorously constrain models that compare well with observations with respect to their PC slopes. For the purpose of this paper, we show the comparison of the the-

oretical PC relations for the computed models with observations from OGLE-IV RR Lyraes, BL Her stars and classical Cepheids in the Galactic bulge, LMC and SMC in Figs. 9, 10 and 11, respectively. There is a good overlap in the PC relations between models and observations from the Galactic bulge, LMC and SMC at both minimum and maximum light. The models have consistent results with observations with respect to both Fourier parameters as well as colour. Subsequently, we use these models to probe the temperature and opacity profiles and to study the distance between the HIF and the stellar photosphere in an attempt to understand the microphysics of the outer envelopes of these pulsating variable stars.



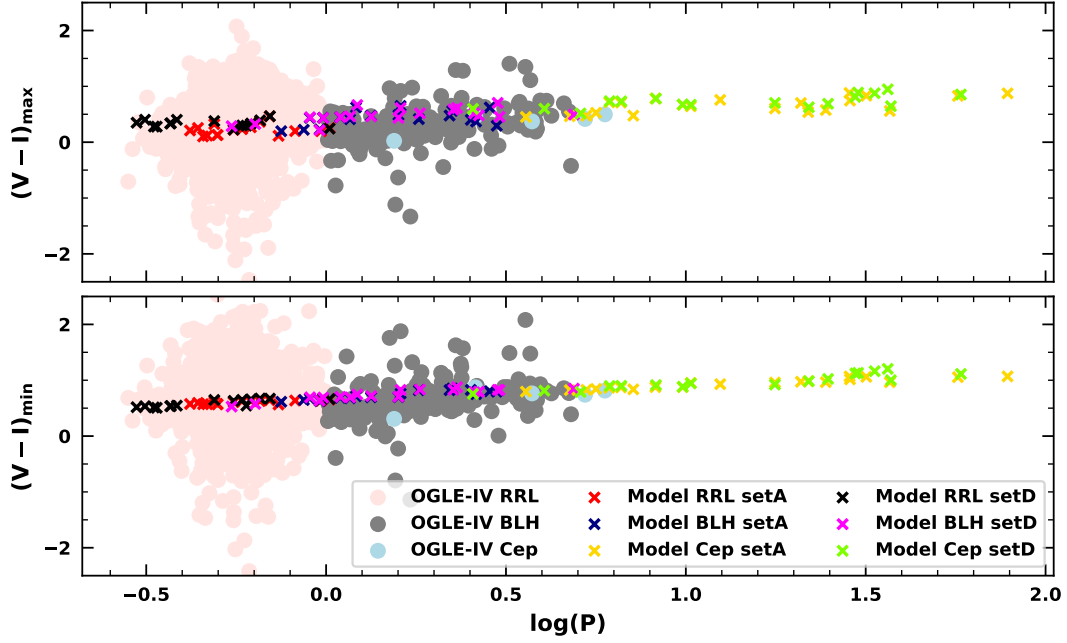


**Figure 9.** A comparison of the theoretical period-colour relations for the computed models with observations from OGLE-IV RR Lyraes, BL Her stars and classical Cepheids in the Galactic bulge.

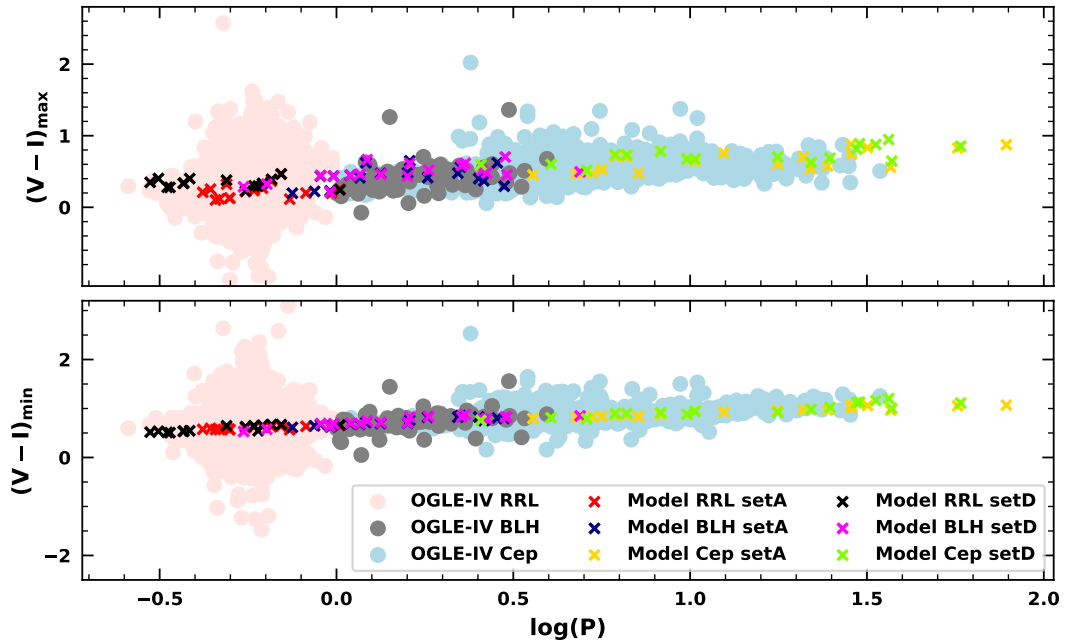


**Figure 10.** Same as Fig. 9 but for observations from LMC.

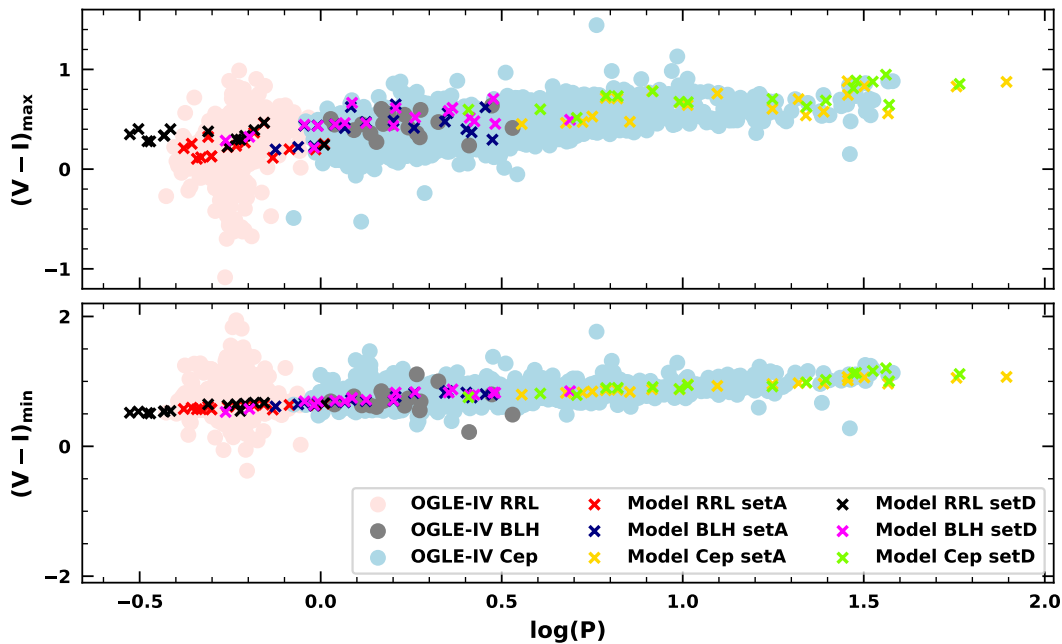


Figure 11. Same as Fig. 9 but for observations from SMC.

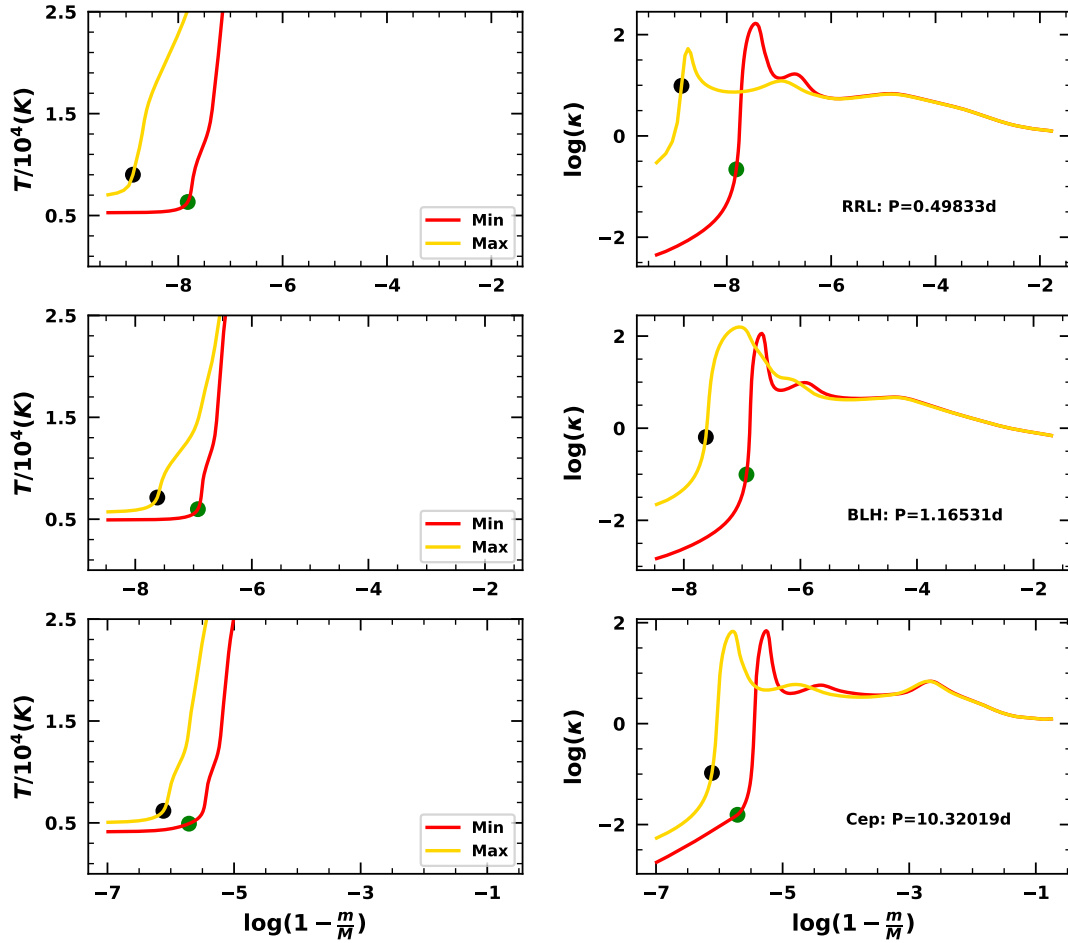
## 5.2 Temperature and opacity profiles

Fig. 12 presents the plots of the temperature and opacity profiles as a function of mass distribution for each of RR Lyrae, BL Her and classical Cepheid models. The mass distribution is measured by the quantity  $Q = \log(1 - M_r/M)$ , where  $M_r$  is the mass within radius,  $r$  and  $M$  is the total mass. The photosphere is defined as the zone with optical depth,  $\tau = 2/3$ . From Fig. 12, we find that the photosphere (shown in filled circles) at maximum light lies further out in the mass distribution than at minimum light; this is expected as the star expands and contracts during its pulsation cycle. However, we observe that the photosphere at maximum light lies much further out in the mass distribution in the case of RR Lyrae ( $Q \sim -9$ ) and BL Her ( $Q \sim -7.5$ ) as compared to Cepheids ( $Q \sim -6$ ). Both the temperature and opacity values increase as we move from Cepheids to BL Her to RR Lyraes at maximum and minimum light. The HIF and stellar photosphere can either be engaged or disengaged. The top two left panels of Fig. 12 show an engaged HIF and photosphere while the bottom left panel depicts an example of where they are not engaged. In fact this panel shows an example of where the HIF and photosphere are engaged at one phase (maximum light) and disengaged at another phase (minimum light). When the HIF and photosphere are disengaged, the temperature of the photosphere and hence the colour of the star is more dependent on global stellar parameters and hence exhibits a relationship with period. When the HIF and photosphere are engaged at low temperature ( $T < 6300\text{K}$ ), the temperature of the photosphere and hence the temperature of the photosphere is somewhat independent of density and hence the relation with period is reduced (e.g. RRab’s at minimum light, Cepheids at maximum light). When the HIF and photosphere are engaged at higher temperature (RR Lyraes at maximum light, overtones), ionization equilibrium is more sensitive to temperature. In this situation, the temperature of the photosphere is the temperature

at which hydrogen ionizes and this has a stronger dependency on period.

## 5.3 HIF-Stellar Photosphere Distance

The HIF is defined as the zone with the steepest gradient in temperature. The distance between the stellar photosphere and HIF,  $\Delta$  may then be defined in terms of  $Q = \log(1 - M_r/M)$ . The interested reader is referred to Fig. 9 of Kanbur et al. (2004) for a clear, pictorial representation. Fig. 13 displays the distance between the HIF and stellar photosphere as a function of  $\log(P)$  for a range of theoretical models from RR Lyraes to BL Hers to classical Cepheids. The error bars are estimated from the coarseness of the grid points around the location of HIF. The top and bottom panels represent the distance between the HIF and stellar photosphere at maximum/minimum light respectively. Firstly we note that at maximum light, the HIF and photosphere are always closer together: the distance between HIF and photosphere is always smaller for a given model at maximum light. For RR Lyraes, the HIF and photosphere are always engaged, but at minimum light, this occurs in a temperature regime for which the ionization of hydrogen is somewhat independent of temperature. Because the HIF and photosphere are engaged, temperature of the photosphere is just the same as the temperature at which hydrogen is ionized and this occurs at a temperature that is somewhat independent of period - hence we have flat/shallow PC relations at minimum light for RRab stars. At maximum light, the star is hotter, the HIF and photosphere are still engaged but in a regime that is more sensitive to temperature changes and hence the temperature of the photosphere, which is still the temperature at which hydrogen ionizes, is more sensitive to global stellar parameters and hence we have PC relation at maximum light for RRab stars. Because the RRc stars are hotter, they exhibit non-flat PC relations at maximum/minimum light.



**Figure 12.** The temperature and opacity profiles for RR Lyrae, BL Her and classical Cepheid models. The filled circles are the location of the photosphere at  $\tau = 2/3$  for each phase. Left panel: temperature profile. Right panel: opacity profile.

Cepheids have higher  $L/M$  ratios and are cooler than RR Lyraes and hence from the work of Kanbur (1995) and Kanbur & Phillips (1996) the HIF lies further inside the mass distribution than in the case for RR Lyraes. The HIF and photosphere are disengaged at minimum light and hence the temperature of the photosphere and hence the colour at minimum light are dependent on stellar parameters and we have PC relation with a significant slope. The HIF and photosphere are engaged at maximum light at low temperature and hence we have flattish PC relation at maximum phase. We may regard BL Her stars as intermediate between Cepheids and RR Lyraes. At minimum light there is sufficient disengagement so that the temperature of the photosphere is somewhat dependent on global stellar parameters and hence period. At maximum light, the situation is similar to maximum light for RRab stars. BL Her stars are cooler and brighter than RR Lyraes. Our analysis from Section 2 and the work of Kanbur (1995) and Kanbur & Phillips (1996) suggest that the HIF is further inside the mass distribution, thus increasing the distance between the HIF and stellar photosphere.

Fig. 13 is broadly consistent with this picture. The top panel shows a fairly constant distance between stellar photosphere and HIF at maximum light across variable star type. An interesting result to note from the top panel is the presence of models with zero or negative distance between the HIF and the stellar photosphere at maximum light - a situation where the photosphere “climbs” up the

HIF. A detailed study of the  $D$  to  $R$  ionization front transition (see Adams & Castor 1979) in Cepheids and RR Lyraes may be useful to analyse this situation. The bottom panel (distance between stellar photosphere and HIF at minimum light) displays a sharp jump in the distance at a period of about  $\log(P) \approx 0.5$  followed by an approximately linear increase with period.

WVir stars are highly adiabatic and this poses some problems for existing stellar pulsation codes - hence we have not used MESA-RSP to model WVir stars. However, since they occupy a similar region of the HR Diagram as classical Cepheids, our contention is that the HIF-stellar photosphere interaction will be similar to that in Cepheids. Figs. 2 and 3 provide strong evidence that as stars move off the HB and upward along the AGB, the relative positions of the HIF and stellar photosphere change in such a way as to make this plausible.

## 6 DISCUSSION AND CONCLUSIONS

We have analysed the largest available dataset of T2Cs in the Bulge, LMC and SMC from the OGLE-IV survey for the first time. We found that there exists a flat PC slope at maximum light for W Vir stars in Bulge, LMC and SMC within  $3\sigma$  uncertainties. This is similar to the flat  $PC_{\max}$  slope observed in long period classical

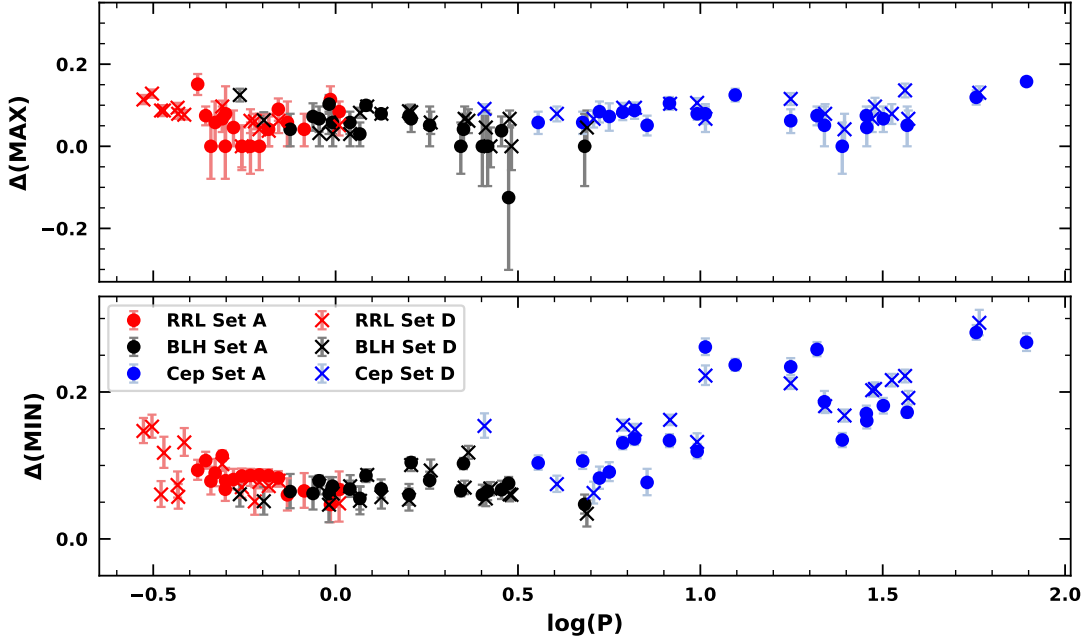


**Figure 13.** The plots of distance ( $\Delta$ ) between HIF and stellar photosphere as function of  $\log(P)$  at maximum and minimum light. The error bars are estimated from the coarseness of the grid points around the location of HIF.

**Table 6.** The slopes and intercepts for PC and AC relations for the RRab, BL Her and classical Cepheid models.

Model	Phase	PC			AC		
		Slope	Intercept	$\sigma$	Slope	Intercept	$\sigma$
Convection set A							
RRab	max	$0.184 \pm 0.206$	$0.265 \pm 0.052$	0.091	$-0.428 \pm 0.032$	$0.635 \pm 0.031$	0.026
	min	$0.181 \pm 0.045$	$0.646 \pm 0.011$	0.02	$-0.072 \pm 0.03$	$0.673 \pm 0.029$	0.024
BLH	max	$0.243 \pm 0.15$	$0.376 \pm 0.039$	0.113	$-0.426 \pm 0.058$	$0.733 \pm 0.046$	0.058
	min	$0.346 \pm 0.044$	$0.668 \pm 0.012$	0.034	$-0.016 \pm 0.076$	$0.74 \pm 0.06$	0.075
Cep	max	$0.252 \pm 0.089$	$0.356 \pm 0.122$	0.101	$-0.497 \pm 0.116$	$1.1 \pm 0.098$	0.082
	min	$0.205 \pm 0.029$	$0.704 \pm 0.039$	0.032	$-0.094 \pm 0.102$	$1.054 \pm 0.086$	0.072
Convection set D							
RRab	max	$-0.036 \pm 0.117$	$0.318 \pm 0.041$	0.063	$-0.14 \pm 0.067$	$0.421 \pm 0.046$	0.054
	min	$0.36 \pm 0.064$	$0.704 \pm 0.022$	0.034	$0.203 \pm 0.055$	$0.458 \pm 0.038$	0.045
BLH	max	$0.289 \pm 0.097$	$0.426 \pm 0.03$	0.097	$-0.35 \pm 0.122$	$0.71 \pm 0.083$	0.098
	min	$0.343 \pm 0.042$	$0.678 \pm 0.013$	0.042	$0.001 \pm 0.116$	$0.743 \pm 0.079$	0.094
Cep	max	$0.213 \pm 0.079$	$0.468 \pm 0.107$	0.087	$-0.092 \pm 0.17$	$0.826 \pm 0.147$	0.113
	min	$0.316 \pm 0.056$	$0.605 \pm 0.076$	0.062	$0.167 \pm 0.183$	$0.881 \pm 0.158$	0.121

Cepheids from present work and [Bhardwaj et al. \(2014\)](#). Also, the  $PC_{\min}$  slope of W Vir stars is much greater than the slope at maximum light. We observed a flat but slightly negative  $PC_{\min}$  slope in BL Her stars from SMC ( $-0.251 \pm 0.339$ ) similar to that obtained for RR Lyrae stars from SMC at minimum light ([Das et al. 2018](#)). The slopes of the PC relations for RV Tau stars in Bulge, LMC and SMC are flat within  $3\sigma$  uncertainties at minimum and maximum light. However, there is high dispersion in all the cases. Using the statistical  $F$ -test, we find a break in the PC relations at a period of 10 days for classical Cepheids in LMC and SMC from

OGLE-IV at both minimum and maximum light, similar to earlier results from [Kanbur & Ngeow \(2004\)](#) and [Bhardwaj et al. \(2014\)](#). There exists a flat  $PC_{\max}$  within  $3\sigma$  uncertainties and a significantly sloped  $PC_{\min}$  for the longer period classical Cepheids in both LMC and SMC. We have also carried out  $t$ -test to study the equivalence of PC slopes in LMC and SMC across a broad spectrum of variable star types and found the results to statistically support the above mentioned results.

We also computed a few RR Lyrae, BL Her and classical Cepheid models using the radial stellar pulsation code in MESA

to theoretically study the distance between HIF and stellar photosphere at minimum and maximum light. We found that RRL models have a flat period-temperature relation at minimum and maximum light within  $3\sigma$  uncertainties using both sets of convection parameters A and D and a flat period-temperature relation at maximum light within  $3\sigma$  uncertainties exists for BL Her and Cepheid models using both sets of convection parameters. The period-temperature relation for the models has a higher dispersion at maximum light than at minimum light. We also found the models to have consistent results with observations with respect to both Fourier parameters as well as colour. The HIF and stellar photosphere are engaged and co-moving at maximum light for classical Cepheids, which results in a flat PC slope at maximum light. However, they are disengaged at minimum light and we observe a significant slope in  $PC_{\min}$ . For RR Lyraes, the HIF and stellar photosphere are engaged during both minimum and maximum light. However, at maximum light, the temperature at which hydrogen starts to ionize appreciably is in a range where Saha ionization equilibrium is much more sensitive to temperature than at the temperatures associated with minimum light, even though the range of densities are similar. This results in a flat  $PC_{\min}$  slope but a significant slope in  $PC_{\max}$ . BL Her stars are cooler and brighter than RR Lyraes; thus we suggest that the HIF is further inside the mass distribution, thereby increasing the distance between the HIF and stellar photosphere. The models computed using MESA are broadly consistent with this picture. We have not computed W Vir stars using MESA; however, similar locations of W Vir stars and classical Cepheids on the HR diagram and similar behaviour of PC relations from observations for both suggest similar HIF and stellar photosphere interaction. Thus, in this work, we have incorporated the PC and AC relations for RR Lyraes, BL Her, W Vir and classical Cepheid stars in a single unifying theory that involves the interaction of the hydrogen ionization front and stellar photosphere and the theory of stellar evolution. Fig. 14 summarizes the main results in the form of a flowchart. An exception to these results are the flat PC relations for BL Her stars at both minimum and maximum light and for W Vir stars at minimum light in the SMC. However, we note here that the statistical sample of stars in the SMC is small ( $\sim 20$  BL Her and  $\sim 15$  W Vir stars).

Paxton et al. (2019) have outlined the physical and numerical assumptions incorporated in the MESA-RSP code and demonstrated that it produces stable, multi-wavelength light curve models for a broad spectrum of variable stars. To evaluate possible systematics in MESA-RSP models due to the input physics such as the equation of state, opacities or color-temperature transformations, it is important to compare these with different pulsation models in the literature. Since MESA-RSP has just been published (Paxton et al. 2019), detailed comparisons between pulsation results with this code and others in the literature have not yet been carried out. We note that comparisons between observations and data for a wide class of radially pulsating stars were reasonable (Paxton et al. 2019). MESA-RSP follows the work of Smolec & Moskalik (2008) in its treatment of stellar pulsation and uses a particular theory of turbulent convection (Kuhfuss 1986). Other similar codes (Marconi et al. 2015) use the convection formulation outlined in Stellingwerf (1982a,b). MESA-RSP affords the possibility of varying the convection parameters used. Using turbulent convection parameter sets A and D (Paxton et al. 2019) suggest that our results are robust to this. In common with other pulsation codes in the literature, MESA-RSP uses the diffusion approximation to account for radiative transfer. Relaxing this assumption is certainly a project for the future but we do not anticipate that a more detailed radiative trans-

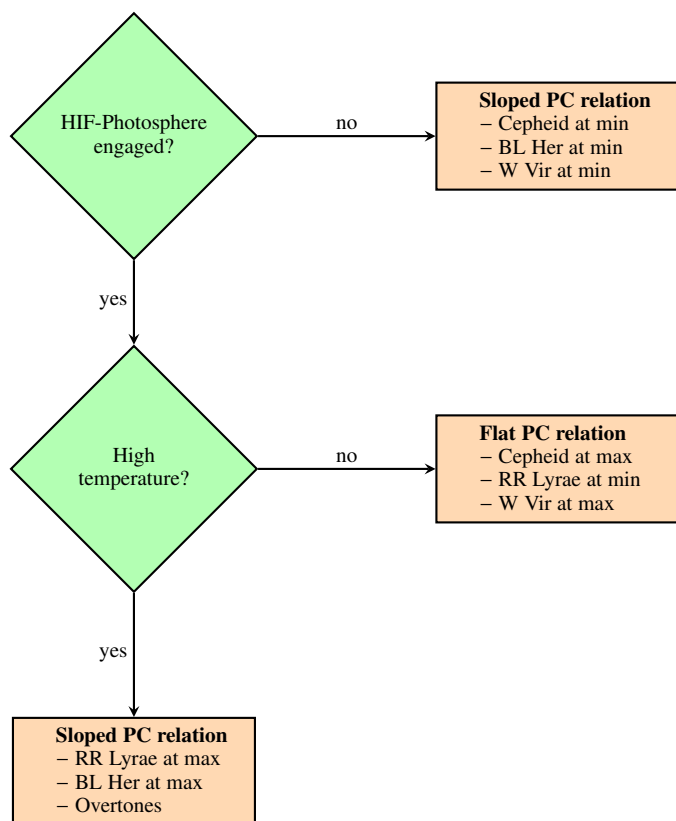


**Figure 14.** A summary of the HIF-stellar photosphere interaction theory explaining the different behaviour of PC relations across a broad spectrum of variable star types at minimum and maximum light.

fer will affect the general character of the results presented here. Previously, Simon et al. (1993) and Kanbur & Phillips (1996) used purely radiative models, whilst Kanbur et al. (2007) and Das et al. (2018) used convection theories from Kuhfuss (1986) and Stellingwerf (1982a), respectively and found similar qualitative results regarding the behaviour of PC relations of classical Cepheids and RR Lyraes. While a detailed comparison of input physics in different pulsation models is beyond the scope of this paper, we are computing a fine grid of Cepheid and RR Lyrae models covering the entire parameter space using MESA-RSP, which will be used to explore possible systematics and constrain pulsation models in the future.

## ACKNOWLEDGEMENTS

The authors thank the referee for useful comments and suggestions that improved the quality of the manuscript. SD acknowledges the INSPIRE Senior Research Fellowship vide Sanction Order No. DST/INSPIRE Fellowship/2016/IF160068 under the INSPIRE Program from the Department of Science & Technology, Government of India. HPS and SMK thank the Indo-US Science and Technology Forum for funding the Indo-US virtual joint networked centre on “Theoretical analyses of variable star light curves in the era of large surveys”. SD acknowledges the travel support provided by SERB, Government of India vide file number ITS/2019/004781 to attend the RR Lyrae/Cepheid 2019 Conference “Frontiers of Classical Pulsators: Theory and Observations”, USA



where the authors had useful discussions. Funding for the Stellar Astrophysics Centre is provided by The Danish National Research Foundation (Grant agreement no.: DNR106). AB acknowledges research grant #11850410434 awarded by the National Natural Science Foundation of China through the Research Fund for International Young Scientists, China Postdoctoral General Grant (2018M640018), and Peking University Strategic Partnership Fund awarded to Peking-Tokyo Joint-collaboration on Research in Astronomy and Astrophysics. BM and NP acknowledge IUSSTF for supporting travel to University of Delhi and AC and RJ thank SUNY Oswego and the NSF STEP grant. The authors acknowledge the use of High Performance Computing facility Pegasus at IUCAA, Pune and the following software used in this project: MESA r10108 and MESA r11701 (Paxton et al. 2011, 2013, 2015, 2018, 2019).

## REFERENCES

- Adams T. F., Castor J. I., 1979, *ApJ*, **230**, 826
- Anderson R. I., Saio H., Ekström S., Georgy C., Meynet G., 2016, *A&A*, **591**, A8
- Angulo C., et al., 1999, *Nuclear Physics A*, **656**, 3
- Bart M. L., 1982, *IMA J. Num. Analysis*, **2**, 241
- Beaton R. L., Carnegie-Chicago Hubble Program Team 2018, in *American Astronomical Society Meeting Abstracts #231*. p. 351.05
- Beaton R. L., et al., 2016, *ApJ*, **832**, 210
- Bellinger E. P., Kanbur S. M., Bhardwaj A., Marconi M., 2019, *MNRAS*, **p. 2948**
- Bhardwaj A., Kanbur S. M., Singh H. P., Ngeow C.-C., 2014, *MNRAS*, **445**, 2655
- Bhardwaj A., Kanbur S. M., Singh H. P., Macri L. M., Ngeow C.-C., 2015, *MNRAS*, **447**, 3342
- Bhardwaj A., Kanbur S. M., Macri L. M., Singh H. P., Ngeow C.-C., Wagner-Kaiser R., Sarajedini A., 2016a, *AJ*, **151**, 88
- Bhardwaj A., Kanbur S. M., Macri L. M., Singh H. P., Ngeow C.-C., Ishida E. E. O., 2016b, *MNRAS*, **457**, 1644
- Bhardwaj A., Macri L. M., Rejkuba M., Kanbur S. M., Ngeow C.-C., Singh H. P., 2017a, *AJ*, **153**, 154
- Bhardwaj A., Kanbur S. M., Marconi M., Rejkuba M., Singh H. P., Ngeow C.-C., 2017b, *MNRAS*, **466**, 2805
- Böhm-Vitense E., 1958, *Z. Astrophys.*, **46**, 108
- Bono G., et al., 2016, *Communications of the Konkoly Observatory Hungary*, **105**, 149
- Cardelli J. A., Clayton G. C., Mathis J. S., 1989, *ApJ*, **345**, 245
- Das S., Bhardwaj A., Kanbur S. M., Singh H. P., Marconi M., 2018, *MNRAS*, **481**, 2000
- Deb S., Singh H. P., 2009, *A&A*, **507**, 1729
- Fadeyev Y. A., 2019, *Astronomy Letters*, **45**, 353
- Fiorentino G., Marconi M., Musella I., Caputo F., 2007, *A&A*, **476**, 863
- Fokin A. B., 1994, *A&A*, **292**, 133
- Gezer I., Van Winckel H., Bozkurt Z., De Smedt K., Kamath D., Hillen M., Manick R., 2015, *MNRAS*, **453**, 133
- Gingold R. A., 1985, *MmSAI*, **56**, 169
- Gonzalez O. A., Rejkuba M., Zoccali M., Valenti E., Minniti D., Schultheis M., Tobar R., Chen B., 2012, *A&A*, **543**, A13
- Grevesse N., Sauval A. J., 1998, *Space Sci. Rev.*, **85**, 161
- Groenewegen M. A. T., Jurkovic M. I., 2017a, *A&A*, **603**, A70
- Groenewegen M. A. T., Jurkovic M. I., 2017b, *A&A*, **604**, A29
- Haschke R., Grebel E. K., Duffau S., 2011, *AJ*, **141**, 158
- Hopf E., 1930, *MNRAS*, **90**
- Iglesias C. A., Rogers F. J., 1996, *ApJ*, **464**, 943
- Iwanek P., et al., 2018, *AcA*, **68**, 213
- Kanbur S. M., 1995, *A&A*, **297**, L91
- Kanbur S. M., Ngeow C.-C., 2004, *MNRAS*, **350**, 962
- Kanbur S. M., Ngeow C.-C., 2006, *MNRAS*, **369**, 705
- Kanbur S. M., Phillips P. M., 1996, *A&A*, **314**, 514
- Kanbur S. M., Ngeow C.-C., Buchler J. R., 2004, *MNRAS*, **354**, 212
- Kanbur S. M., Ngeow C.-C., Feiden G., 2007, *MNRAS*, **380**, 819
- Kuhfuss R., 1986, *A&A*, **160**, 116
- Manick R., Van Winckel H., Kamath D., Hillen M., Escorza A., 2017, *A&A*, **597**, A129
- Marconi M., Di Criscienzo M., 2007, *A&A*, **467**, 223
- Marconi M., Molinaro R., Ripepi V., Musella I., Brocato E., 2013, *MNRAS*, **428**, 2185
- Marconi M., et al., 2015, *ApJ*, **808**, 50
- Matsunaga N., et al., 2013, *MNRAS*, **429**, 385
- Muraveva T., et al., 2015, *ApJ*, **807**, 127
- Nataf D. M., et al., 2013, *ApJ*, **769**, 88
- Ngeow C.-C., Sarkar S., Bhardwaj A., Kanbur S. M., Singh H. P., 2015, *ApJ*, **813**, 57
- Ngeow C.-C., Kanbur S. M., Bhardwaj A., Schreengost Z., Singh H. P., 2017, *ApJ*, **834**, 160
- Nishiyama S., Tamura M., Hatano H., Kato D., Tanabé T., Sugitani K., Nagata T., 2009, *ApJ*, **696**, 1407
- Paxton B., Bildsten L., Dotter A., Herwig F., Lesaffre P., Timmes F., 2011, *ApJS*, **192**, 3
- Paxton B., et al., 2013, *ApJS*, **208**, 4
- Paxton B., et al., 2015, *ApJS*, **220**, 15
- Paxton B., et al., 2018, *ApJS*, **234**, 34
- Paxton B., et al., 2019, *ApJS*, **243**, 10
- Popowski P., 2000, *ApJL*, **528**, L9
- Preston G. W., 1964, *ARA&A*, **2**, 23
- Reimers D., 1975, *Memoires of the Societe Royale des Sciences de Liege*, **8**, 369
- Riess A. G., et al., 2016, *ApJ*, **826**, 56
- Riess A. G., Casertano S., Yuan W., Macri L. M., Scolnic D., 2019, *ApJ*, **876**, 85
- Ripepi V., et al., 2017, *MNRAS*, **472**, 808
- Rogers F. J., Nayfonov A., 2002, *ApJ*, **576**, 1064
- Sandage A., Tammann G. A., 2006, *ARA&A*, **44**, 93
- Schlegel D. J., Finkbeiner D. P., Davis M., 1998, *ApJ*, **500**, 525
- Simon N. R., Kanbur S. M., Mihalas D., 1993, *ApJ*, **414**, 310
- Smolec R., 2016, *MNRAS*, **456**, 3475
- Smolec R., Moskalik P., 2008, *AcA*, **58**, 193
- Smolec R., et al., 2012, *MNRAS*, **419**, 2407
- Smolec R., Moskalik P., Plachy E., Soszyński I., Udalski A., 2018, *MNRAS*, **481**, 3724
- Soszyński I., et al., 2008, *AcA*, **58**, 293
- Soszyński I., et al., 2015, *Acta Astron.*, **65**, 297
- Soszyński I., et al., 2017, *AcA*, **67**, 297
- Soszyński I., et al., 2018, *AcA*, **68**, 89
- Soszyński I., Smolec R., Udalski A., Pietrukowicz P., 2019, *ApJ*, **873**, 43
- Stellingwerf R. F., 1982a, *ApJ*, **262**, 330
- Stellingwerf R. F., 1982b, *ApJ*, **262**, 339
- Subramanian S., Marengo M., Bhardwaj A., Huang Y., Inno L., Nakagawa A., Storm J., 2017, *Space Sci. Rev.*, **212**, 1817
- Tammann G. A., Sandage A., Reindl B., 2003, *A&A*, **404**, 423
- Tuchman Y., Lebre A., Mennessier M. O., Yarrı A., 1993, *A&A*, **271**, 501
- Udalski A., 2003, *ApJ*, **590**, 284
- Wallerstein G., 2002, *PASP*, **114**, 689

## APPENDIX A: STATISTICAL *T*-TEST TABLES

The results from the statistical *t*-test to compare PC slopes in the LMC and SMC across a broad spectrum of variable star types are summarised in Tables A1 and A2, respectively and discussed in Sec. 4.2.3.

**Table A1.** Results of  $t$ -test on PC slopes in the LMC\*.

	BL Her	W Vir	pW Vir	RV Tau	T2C	RRab	Cep <sub>S</sub>	Cep <sub>L</sub>	Cep <sub>all</sub>
Minimum light									
BL Her	...	...	...	...	...	...	...	...	...
W Vir	(0.055,1.975,0.478)	...	...	...	...	...	...	...	...
pW Vir	(0.508,1.987,0.306)	(0.500,1.982,0.309)	...	...	...	...	...	...	...
RV Tau	(1.485,1.981,0.070)	(1.487,1.977,0.070)	(1.068,1.994,0.145)	...	...	...	...	...	...
T2C	<b>(3.787,1.968,0.000)</b>	<b>(5.045,1.967,0.000)</b>	(1.015,1.969,0.156)	(0.657,1.968,0.256)	...	...	...	...	...
RRab	<b>(4.321,1.960,0.000)</b>	<b>(5.877,1.960,0.000)</b>	(1.200,1.960,0.115)	(0.558,1.960,0.288)	(1.546,1.960,0.061)	...	...	...	...
Cep <sub>S</sub>	<b>(3.575,1.961,0.000)</b>	<b>(4.878,1.961,0.000)</b>	(0.889,1.961,0.187)	(0.730,1.961,0.233)	(1.216,1.961,0.112)	<b>(4.825,1.960,0.000)</b>	...	...	...
Cep <sub>L</sub>	(0.399,1.973,0.345)	(0.421,1.972,0.337)	(0.343,1.978,0.366)	(1.399,1.975,0.082)	<b>(4.765,1.967,0.000)</b>	<b>(5.650,1.960,0.000)</b>	<b>(4.588,1.961,0.000)</b>	...	...
Cep <sub>all</sub>	<b>(3.114,1.961,0.001)</b>	<b>(4.242,1.961,0.000)</b>	(0.703,1.961,0.241)	(0.832,1.961,0.203)	<b>(2.991,1.961,0.001)</b>	<b>(7.991,1.960,0.000)</b>	<b>(4.761,1.961,0.000)</b>	<b>(3.909,1.961,0.000)</b>	...
Mean light									
BL Her	...	...	...	...	...	...	...	...	...
W Vir	<b>(4.523,1.976,0.000)</b>	...	...	...	...	...	...	...	...
pW Vir	(0.271,1.988,0.394)	(1.567,1.982,0.060)	...	...	...	...	...	...	...
RV Tau	<b>(2.309,1.981,0.011)</b>	(1.002,1.978,0.159)	<b>(1.774,1.994,0.040)</b>	...	...	...	...	...	...
T2C	<b>(5.878,1.968,0.000)</b>	(0.087,1.967,0.465)	(1.598,1.969,0.056)	(1.039,1.968,0.150)	...	...	...	...	...
RRab	(0.277,1.960,0.391)	<b>(6.690,1.960,0.000)</b>	(0.369,1.960,0.356)	<b>(2.420,1.960,0.008)</b>	<b>(17.059,1.960,0.000)</b>	...	...	...	...
Cep <sub>S</sub>	<b>(5.811,1.961,0.000)</b>	(0.412,1.961,0.340)	(1.510,1.961,0.066)	(1.108,1.961,0.134)	(0.887,1.961,0.188)	<b>(25.542,1.960,0.000)</b>	...	...	...
Cep <sub>L</sub>	<b>(1.905,1.973,0.029)</b>	<b>(2.544,1.972,0.006)</b>	(0.522,1.977,0.301)	<b>(1.741,1.974,0.042)</b>	<b>(3.253,1.967,0.001)</b>	<b>(2.899,1.960,0.002)</b>	<b>(3.079,1.961,0.001)</b>	...	...
Cep <sub>all</sub>	<b>(5.526,1.961,0.000)</b>	(0.733,1.961,0.232)	(1.416,1.961,0.078)	(1.174,1.961,0.120)	<b>(1.823,1.961,0.034)</b>	<b>(26.072,1.960,0.000)</b>	<b>(1.782,1.961,0.037)</b>	<b>(2.789,1.961,0.003)</b>	...
Maximum light									
BL Her	...	...	...	...	...	...	...	...	...
W Vir	<b>(3.538,1.975,0.000)</b>	...	...	...	...	...	...	...	...
pW Vir	(0.979,1.986,0.165)	<b>(3.325,1.982,0.001)</b>	...	...	...	...	...	...	...
RV Tau	<b>(1.987,1.980,0.025)</b>	(0.170,1.978,0.433)	<b>(2.397,1.995,0.010)</b>	...	...	...	...	...	...
T2C	(1.619,1.968,0.053)	<b>(3.409,1.967,0.000)</b>	<b>(2.020,1.969,0.022)</b>	(1.359,1.968,0.088)	...	...	...	...	...
RRab	<b>(11.648,1.960,0.000)</b>	<b>(19.370,1.960,0.000)</b>	<b>(5.380,1.960,0.000)</b>	<b>(8.460,1.960,0.000)</b>	<b>(47.812,1.960,0.000)</b>	...	...	...	...
Cep <sub>S</sub>	(0.685,1.961,0.247)	<b>(4.637,1.961,0.000)</b>	(1.496,1.961,0.067)	<b>(1.877,1.961,0.030)</b>	<b>(3.601,1.961,0.000)</b>	<b>(57.780,1.960,0.000)</b>	...	...	...
Cep <sub>L</sub>	<b>(3.922,1.973,0.000)</b>	(0.457,1.972,0.324)	<b>(3.585,1.977,0.000)</b>	(0.431,1.974,0.334)	<b>(3.963,1.967,0.000)</b>	<b>(19.626,1.960,0.000)</b>	<b>(5.178,1.961,0.000)</b>	...	...
Cep <sub>all</sub>	(1.410,1.961,0.079)	<b>(3.798,1.961,0.000)</b>	<b>(1.898,1.961,0.029)</b>	(1.495,1.961,0.068)	(0.962,1.961,0.168)	<b>(67.469,1.960,0.000)</b>	<b>(4.085,1.961,0.000)</b>	<b>(4.358,1.961,0.000)</b>	...

\* Values in parentheses are (T,  $t_{\alpha/2, \nu}$ , p-value). The bold-faced entries indicate that the null hypothesis of the equivalent PC slopes can be rejected.

**Table A2.** Results of  $t$ -test on PC slopes in the SMC\*.

	BL Her	W Vir	pW Vir	RV Tau	T2C	RRab	Cep <sub>S</sub>	Cep <sub>L</sub>	Cep <sub>all</sub>
Minimum light									
BL Her	...	...	...	...	...	...	...	...	...
W Vir	(1.682,2.040,0.051)	...	...	...	...	...	...	...	...
pW Vir	(1.404,2.069,0.087)	(0.449,2.101,0.329)	...	...	...	...	...	...	...
RV Tau	(0.213,2.056,0.416)	(1.509,2.080,0.073)	(1.416,2.160,0.090)	...	...	...	...	...	...
T2C	(1.288,1.995,0.101)	(1.278,1.998,0.103)	(0.787,2.004,0.217)	(1.204,2.002,0.117)	...	...	...	...	...
RRab	(0.383,1.961,0.351)	<b>(4.082,1.961,0.000)</b>	(1.447,1.961,0.074)	(0.541,1.961,0.294)	<b>(4.758,1.961,0.000)</b>	...	...	...	...
Cep <sub>S</sub>	(1.315,1.961,0.094)	(1.401,1.961,0.081)	(0.785,1.961,0.216)	(1.220,1.961,0.111)	(0.060,1.961,0.476)	<b>(8.958,1.960,0.000)</b>	...	...	...
Cep <sub>L</sub>	<b>(2.247,1.981,0.013)</b>	(1.395,1.982,0.083)	(0.093,1.984,0.463)	<b>(1.908,1.983,0.030)</b>	<b>(4.061,1.976,0.000)</b>	<b>(9.331,1.961,0.000)</b>	<b>(5.474,1.961,0.000)</b>	...	...
Cep <sub>all</sub>	(1.399,1.961,0.081)	(1.140,1.961,0.127)	(0.725,1.961,0.234)	(1.282,1.961,0.100)	(0.574,1.961,0.283)	<b>(9.813,1.960,0.000)</b>	<b>(3.626,1.960,0.000)</b>	<b>(5.002,1.961,0.000)</b>	...
Mean light									
BL Her	...	...	...	...	...	...	...	...	...
W Vir	(0.828,2.040,0.207)	...	...	...	...	...	...	...	...
pW Vir	(1.408,2.069,0.086)	(1.075,2.101,0.148)	...	...	...	...	...	...	...
RV Tau	(0.221,2.056,0.413)	(0.780,2.080,0.222)	(1.360,2.160,0.098)	...	...	...	...	...	...
T2C	(1.301,1.995,0.099)	(0.890,1.998,0.188)	(0.865,2.004,0.195)	(1.056,2.002,0.148)	...	...	...	...	...
RRab	<b>(3.571,1.961,0.000)</b>	<b>(6.028,1.961,0.000)</b>	(0.411,1.961,0.341)	<b>(2.434,1.961,0.007)</b>	<b>(10.733,1.961,0.000)</b>	...	...	...	...
Cep <sub>S</sub>	(1.461,1.961,0.072)	(1.284,1.961,0.100)	(0.791,1.961,0.215)	(1.146,1.961,0.126)	(0.733,1.961,0.232)	<b>(21.038,1.960,0.000)</b>	...	...	...
Cep <sub>L</sub>	<b>(2.549,1.981,0.006)</b>	<b>(3.408,1.982,0.000)</b>	(0.125,1.984,0.450)	<b>(1.837,1.983,0.035)</b>	<b>(4.052,1.976,0.000)</b>	<b>(3.367,1.961,0.000)</b>	<b>(4.417,1.961,0.000)</b>	...	...
Cep <sub>all</sub>	(1.544,1.961,0.061)	(1.474,1.961,0.070)	(0.745,1.961,0.228)	(1.196,1.961,0.116)	(1.172,1.961,0.121)	<b>(20.419,1.960,0.000)</b>	<b>(2.526,1.960,0.006)</b>	<b>(4.114,1.961,0.000)</b>	...
Maximum light									
BL Her	...	...	...	...	...	...	...	...	...
W Vir	(0.574,2.040,0.285)	...	...	...	...	...	...	...	...
pW Vir	(1.346,2.069,0.096)	<b>(1.810,2.101,0.044)</b>	...	...	...	...	...	...	...
RV Tau	(0.473,2.056,0.320)	(0.823,2.080,0.210)	(0.551,2.160,0.295)	...	...	...	...	...	...
T2C	(0.967,1.995,0.168)	<b>(1.942,1.998,0.028)</b>	(0.963,2.004,0.170)	(0.051,2.002,0.480)	...	...	...	...	...
RRab	<b>(9.782,1.961,0.000)</b>	<b>(11.910,1.961,0.000)</b>	<b>(4.618,1.961,0.000)</b>	<b>(4.252,1.961,0.000)</b>	<b>(32.049,1.961,0.000)</b>	...	...	...	...
Cep <sub>S</sub>	(1.607,1.961,0.054)	<b>(2.695,1.961,0.004)</b>	(0.580,1.961,0.281)	(0.249,1.961,0.402)	<b>(3.011,1.961,0.001)</b>	<b>(40.785,1.960,0.000)</b>	...	...	...
Cep <sub>L</sub>	(0.769,1.981,0.222)	<b>(1.667,1.982,0.049)</b>	(1.052,1.983,0.148)	(0.131,1.983,0.448)	(0.421,1.976,0.337)	<b>(22.623,1.961,0.000)</b>	<b>(2.221,1.961,0.013)</b>	...	...
Cep <sub>all</sub>	(1.524,1.961,0.064)	<b>(2.601,1.961,0.005)</b>	(0.632,1.961,0.264)	(0.209,1.961,0.417)	<b>(2.642,1.961,0.004)</b>	<b>(41.800,1.960,0.000)</b>	(1.170,1.960,0.121)	<b>(1.995,1.961,0.023)</b>	...

\* Values in parentheses are (T,  $t_{\alpha/2, \nu}$ , p-value). The bold-faced entries indicate that the null hypothesis of the equivalent PC slopes can be rejected.